Electromagnetic Information Theory for Holographic MIMO Communications

Li Wei, *Member, IEEE*, Tierui Gong, *Member, IEEE*, Chongwen Huang, *Senior Member, IEEE*, Zhaoyang Zhang, *Senior Member, IEEE*, Wei E. I. Sha, *Fellow, IEEE*, Zhi Ning Chen, *Fellow, IEEE*, Linglong Dai, *Fellow, IEEE*, Mérouane Debbah, *Fellow, IEEE*, and Chau Yuen, *Fellow, IEEE*

***Abstract*—Holographic multiple-input multiple-output (HMIMO) has recently emerged as a key enabler for next-generation wireless systems due to its capability to form nearly continuous apertures, enabling ultra-high spatial resolution and significantly enhanced capacity. However, this paradigm also raises fundamental questions about the applicability of Shannon's information theory (SIT) to HMIMO systems and whether physical constraints—such as aperture size, electromagnetic (EM) coupling, resonance, and wavefront curvature—introduce additional limits beyond conventional statistical models. Classical SIT focuses on the probabilistic input–output relationship but does not explicitly incorporate the EM field interactions that fundamentally govern wave propagation. To bridge this gap, this paper introduces an electromagnetic information theory (EIT) framework for HMIMO systems, which unifies EM field theory with both Shannon's probabilistic and Kolmogorov's functional formulations of information theory to establish a physically consistent and mathematically complete foundation for performance evaluation. The paper establishes the fundamental physical limits—including constraints on antenna design, gain, and beamwidth—and examines their implications for HMIMO implementations. It then characterizes the excitation–field relationship and the corresponding field sampling and spatial degrees of freedom under physical constraints. Subsequently, field-based and operator-theoretic channel models are developed to describe EM-compliant propagation in HMIMO systems. By combining the statistical representation of SIT with the functional representation of Kolmogorov's information theory, the proposed EIT framework provides a unified perspective on channel capacity, information flow, and field representation. Finally, we outline open research directions, including EM environment control, 3D superdirective HMIMO design, efficient field sampling, scattering and EM noise modeling, and excitation/field-based encoding and modulation. These developments mark a paradigm shift toward physically grounded, high-capacity, and adaptive wireless communication systems empowered by HMIMO and EIT.**

***Index Terms*—Holographic multiple-input multiple-output (HMIMO), antenna theory, cannel modeling, electromagnetic wave theory, information theory.**

Received 31 January 2026; revised 5 April 2026; accepted 16 April 2026. Date of publication 4 May 2026; date of current version 15 May 2026. This work was supported in part by the Ministry of Education (MOE), Singapore, through MOE Tier 2 under Award T2EP50124-0032; in part by China National Key Research and Development Program under Grant 2021YFA1000500, Grant 2025ZD1301900, and Grant 2023YFB2904804; in part by the National Natural Science Foundation of China under Grant 62331023 and Grant 62394292; in part by Zhejiang Provincial Natural Science Foundation for Distinguished Young Scholars under Grant LRG26F010001; and in part by the Fundamental Research Funds for the Central Universities and Zhejiang University Global Partnership Fund. *(Corresponding author: Chau Yuen.)*

Li Wei is with the College of Information Science and Electronic Engineering, Zhejiang University, Hangzhou 310027, China, and also with the School of Electrical and Electronics Engineering, Nanyang Technological University, Singapore 639798 (e-mail: weili_xd@163.com).

Tierui Gong and Chau Yuen are with the School of Electrical and Electronics Engineering, Nanyang Technological University, Singapore 639798 (e-mail: trgTerry1113@gmail.com; chau.yuen@ntu.edu.sg).

Chongwen Huang and Zhaoyang Zhang are with the College of Information Science and Electronic Engineering, Zhejiang Provincial Key Laboratory of Multi-Modal Communication Networks and Intelligent Information Processing, and the National Key Laboratory of Millimeter-Wave and Terahertz Remote Sensing, Zhejiang University, Hangzhou 310027, China (e-mail: chongwenhuang@zju.edu.cn; ning_ming@zju.edu.cn).

Wei E. I. Sha is with the College of Information Science and Electronic Engineering, Zhejiang University, Hangzhou 310027, China (e-mail: weisha@zju.edu.cn).

Zhi Ning Chen is with the Department of Electrical and Computer Engineering, National University of Singapore, Singapore 117583 (e-mail: eleczn@nus.edu.sg).

Linglong Dai is with Beijing National Research Center for Information Science and Technology and the Department of Electronic Engineering, Tsinghua University, Beijing 100084, China (e-mail: daill@tsinghua.edu.cn).

Mérouane Debbah is with the Research Institute for Digital Future, Khalifa University, Abu Dhabi, United Arab Emirates (e-mail: merouane.debbah@ku.ac.ae).

Digital Object Identifier 10.1109/COMST.2026.3689548

I. Introduction

THE integration of electromagnetic (EM) theory with information theory has recently attracted significant attention in wireless communications, as it provides a unified physical and informational perspective for analyzing the fundamental limits of communication systems. Although EM wave interactions are well-understood in the EM community, the integration of EM wave theory in wireless communications is still in the early stages. In the majority of theoretical analyses in wireless communications, multiple assumptions are adopted to relieve the analytical and computational burdens, which may be far from the practical bound in applications. This situation has worsened in recent years, as the emergence of new technologies—driven by advances in fabrication and low-profile materials—has rendered many assumptions valid in traditional communications no longer applicable, especially in the context of compact antenna arrays and near-field communications. Therefore, exploring the fundamental limits of such scenarios forces us to go back and review the EM wave theory. By inspecting the physical limitations, e.g., quality factor and effective radiation gain, which are typically overlooked in performance analysis in wireless communications, a theoretical framework with a trade-off between numerical complexity and performance evaluation is anticipated to be provided.

1553-877X © 2026 IEEE. All rights reserved, including rights for text and data mining, and training of artificial intelligence and similar technologies. Personal use is permitted, but republication/redistribution requires IEEE permission.
See https://www.ieee.org/publications/rights/index.html for more information.

Authorized licensed use limited to: Zhejiang University. Downloaded on May 24,2026 at 03:23:22 UTC from IEEE Xplore. Restrictions apply.

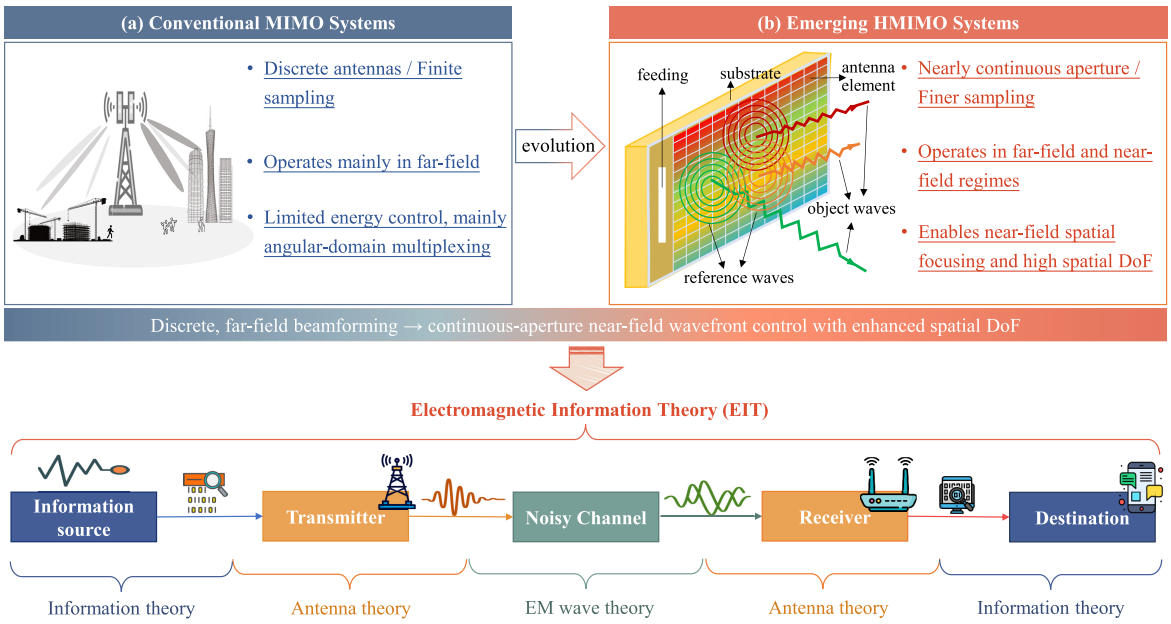

Fig. 1. Unified depiction of MIMO–HMIMO evolution and the formation of EIT as a bridging framework.

A. Development of Holographic MIMO Systems

The traditional multiple-input multiple-output (MIMO) systems enable simultaneous and independent data transmission to serve a larger number of users, which is achieved by spatially separating multiple antennas with spacing larger than half of the wavelength to ensure channel independence, as shown in Fig. 1 (a). Since the number of mobile devices is growing dramatically and the communication scenarios have diversified these years, the traditional MIMO systems remain mainly two problems: one is the impracticality of accommodating multiple-antenna arrays in a constrained region, e.g., portable devices, and the other one is the high cost of achieving full coverage. To deal with the former problem, compact antenna arrays with few low-profile antennas (e.g., two or four antennas) are proposed to be housed in small terminals [1], [2], [3]. To further support full coverage, a larger array size with more compact antenna elements is proposed, i.e., tightly coupled antenna arrays [4], [5]. However, the serious coupling effects and reduced radiation efficiency are unavoidable in compact antenna arrays. Therefore, some methods (e.g., employing decorrelation techniques, involving matching networks) are proposed to preserve MIMO channel capacity in compact antenna arrays.

With the development of fabrication techniques and novel metamaterials, the concept of incorporating a large number of low-cost and electrically small antenna elements within physically constrained apertures has emerged, giving rise to holographic multiple-input multiple-output (HMIMO) systems [6], [7], [8], [9], [10], [11]. As illustrated in Fig. 1, traditional MIMO systems employ discrete antenna elements that provide only finite spatial sampling, operate mainly in the far-field regime, and offer limited control over spatial energy distribution. In principle, HMIMO aims to realize a nearly continuous-aperture transceiver surface, where densely packed sub-wavelength elements collaboratively synthesize desired radiation patterns through intelligent current distribution. It is important to distinguish HMIMO from reconfigurable intelligent surfaces (RIS) [12], [13], [14]. A RIS is typically a passive or semi-passive surface that modifies the propagation environment via tunable reflections but does not actively generate or receive baseband signals. In contrast, HMIMO is envisioned as an active transceiver architecture capable of directly generating, modulating, and receiving EM fields—thereby enabling full exploitation of spatial and modal degrees of freedom (DoF). Although such continuous-aperture transceivers have not yet been realized in practical wireless systems, they are expected to enable near-field wavefront synthesis and spatial focusing, with the potential for higher spatial DoF, improved energy efficiency, and extended functionality in sensing, positioning, and imaging.

Despite their shared objective of improving communication performance, antenna engineering and wireless communications often adopt distinct modeling perspectives for HMIMO systems. Antenna engineers typically analyze current distributions, impedance matching, mutual coupling, and radiation efficiency from an EM standpoint, whereas communication theorists focus on capacity, spectral efficiency, and channel statistics using abstract propagation models. This difference in focus leads to a conceptual gap between the physical modeling paradigm and the information-theoretic paradigm. Consequently, a physics-consistent framework is needed to unify the performance metrics across both domains and reveal how physical constraints on EM waves fundamentally determine achievable information transfer in HMIMO systems.

B. Electromagnetic Information Theory

The remarkable capability of HMIMO systems to manipulate EM fields provides unprecedented flexibility for future wireless networks. However, traditional communication theories built upon Shannon's information theory (SIT) [15]

Authorized licensed use limited to: Zhejiang University. Downloaded on May 24,2026 at 03:23:22 UTC from IEEE Xplore. Restrictions apply.

describe information transmission in purely probabilistic terms, without explicitly considering EM field interactions, mutual coupling, or spatial wave phenomena that arise in large-aperture and near-field systems. Therefore, to achieve physically consistent performance characterization and system design, it is essential to establish a unified framework—electromagnetic information theory (EIT)—that integrates EM field theory with information-theoretic principles.

The concept of EIT can be traced back to the 1940s [16], [17] when Gabor first indicated that communications are interpretations of physical effects. Shannon then proposed probabilistic models for communications in [15] and Kolmogorov introduced functional sets for information measurement in [18]. Later, in the 1980s, Bucci and Franceschetti shaped the concept of spatial bandwidth and explored the DoF of scattered fields [19], [20], which were then extended to the arbitrary surfaces in the 1990s [21]. Subsequently, in the 2000s, Miller et al. investigated the DoF and power coupling strengths for optical systems [22], [23]; Poon et al. explored the DoF in multiantenna channels [24]; Migliore examined the DoF of the wave field in MIMO channels [25] and bridged electromagnetics and information theory via using the Kolmogorov approach [26]; and Franceschetti et al. investigated information-theoretic limits of wireless communication problems in a deterministic structure [27]. In [28], the Shannon information capacity of space-time wireless channels is derived with physical constraints. More works on the relationship between DoF of wireless networks and physics are discussed in [29]. Although a long history EIT possesses, the research interest is still growing in the 2020s as many authors were dedicated to this interdisciplinary discourse in multiple fields [30], [31], [32], [33], [34], [35], [36], [37], [38], [39], [40], [41].

Undoubtedly, EIT serves as an effective interdisciplinary framework to evaluate HMIMO communications with proper integration of information theory and EM wave theory [26], [30], [31]. It models the communication systems by taking into account the physical effects of EM wave propagation, resulting in both probabilistic model and deterministic model, which is more physically consistent than the probabilistic only framework that is widely adopted in wireless communications. Particularly, EIT views the wireless channel as a continuous vector wave field excited by an impulse response, which is jointly described by time, frequency, space, polarization, and even orbital angular momentum with each dimension being capable of information-carrying. This interpretation of wireless channel enables EIT to capture the fully-dimensional information, and thus to assist communications for possibly providing higher multiplexing and diversity. Overall, the emergence and development of EIT will potentially allow us to unveil the fundamental limits and perform system designs for HMIMO systems effectively and more realistically.

However, the involvement of EIT in HMIMO communications is still in its infancy. On the one hand, an integrated theoretical framework is still in development because the SIT and EM wave theory are normally investigated in two separate frameworks. On the other hand, the investigations on HMIMO communications encompass not only the propagation environment but also the interactions between antenna surfaces. As such, HMIMO-oriented EIT should consider all these aspects to offer a completed, physically consistent, and effective framework.

To this aim, the physical limitations in HMIMO systems, especially those relevant to antenna designs, should be explored to shed more light on the interactions between EM waves and antenna surfaces. The HMIMO-assisted oversampling techniques are also fascinating as an efficient method for improving spectral efficiency and capacity. Furthermore, the EM-compliant channel modeling in HMIMO systems, examining both the near-field and far-field characteristics, should be built to capture the essence of EM wave propagation, which becomes crucial for both theoretical analyses and system designs. In the EIT framework, the two information measurements, i.e., Shannon capacity [42] and Kolmogorov ϵ-capacity [18], stand out. Shannon capacity is introduced as an effective measurement of information in the probabilistic model while Kolmogorov ϵ-capacity evaluates the amount of information of signals with ϵ accuracy using functional analysis. Based on these two information measurements, the inherent capacity/DoF performance of HMIMO systems is discussed. The comparison of related magazines, surveys, and tutorials is presented in Table I. Although several references in Table I touch on related topics, most surveys, tutorials, and magazines provide only high-level descriptions or brief discussions without in-depth mathematical interpretation or communication-level extension, i.e., the coverage is often introductory and not systematic, stopping at conceptual observations.

In this article, we present a comprehensive review of HMIMO-oriented EIT. The overall structure of the paper is illustrated in Fig. 2. Specifically, the "Fundamental Physical Limits in HMIMO-Oriented EIT" section introduces the intrinsic constraints in HMIMO antenna design, aiming to provide EM interpretations for MIMO systems, including directivity gain, quality factor, and embedded efficiency. The "EM Field Characterization in HMIMO-Oriented EIT" section reviews the Green's function representation of EM fields, discusses two common field assumptions, and highlights the superdirectivity phenomenon in HMIMO systems. The "Field Sampling and DoF under Physical Limits" section presents the characterization of field-sampling and HMIMO-assisted oversampling techniques. The "Channel Modeling within the EIT Framework" section describes different types of EM-compliant channel models, including both field-based and operator-theoretic channel representations. The "Information-Theoretic Foundations for HMIMO-Oriented EIT" section introduces both the probabilistic SIT and the deterministic Kolmogorov information theory (KIT) to quantify the EM information context and discusses the reinterpretation of DoF in HMIMO systems. The "Numerical Evaluation" section presents DoF and capacity analyses based on the SIT and KIT frameworks through simulations. Subsequently, potential research directions are explored in the "Future Research Directions" section. Finally, the article concludes with the "Conclusions" section.

Authorized licensed use limited to: Zhejiang University. Downloaded on May 24,2026 at 03:23:22 UTC from IEEE Xplore. Restrictions apply.

TABLE I
COMPARISON WITH RELATED MAGAZINES/SURVEYS/TUTORIALS

Category	Topic	[8]	[38]	[39]	[40]	[43]	[44]	[45]	[46]	[47]	[48]	[49]	This work
Physical limits	Size-bandwidth tradeoff											✓	✓
	Size-directivity bound												✓
	Coupling effects	✓	✓	✓	✓		✓	✓	✓	✓		✓	✓
EM propagation	Field representation	✓	✓					✓		✓	✓	✓	✓
	Superdirectivity		✓				✓						✓
Sampling & DoF	Field sampling	✓	✓				✓	✓	✓	✓		✓	✓
	DoF characterization	✓	✓	✓		✓		✓	✓	✓	✓	✓	✓
	Spatial oversampling												✓
Channel modeling	Field-based EM model	✓	✓	✓			✓			✓	✓	✓	✓
	Operator-theoretical model			✓		✓		✓	✓				✓
Theoretical analysis	Shannon's information theory	✓	✓	✓	✓		✓	✓		✓	✓	✓	✓
	Kolmogorov information theory						✓	✓					✓

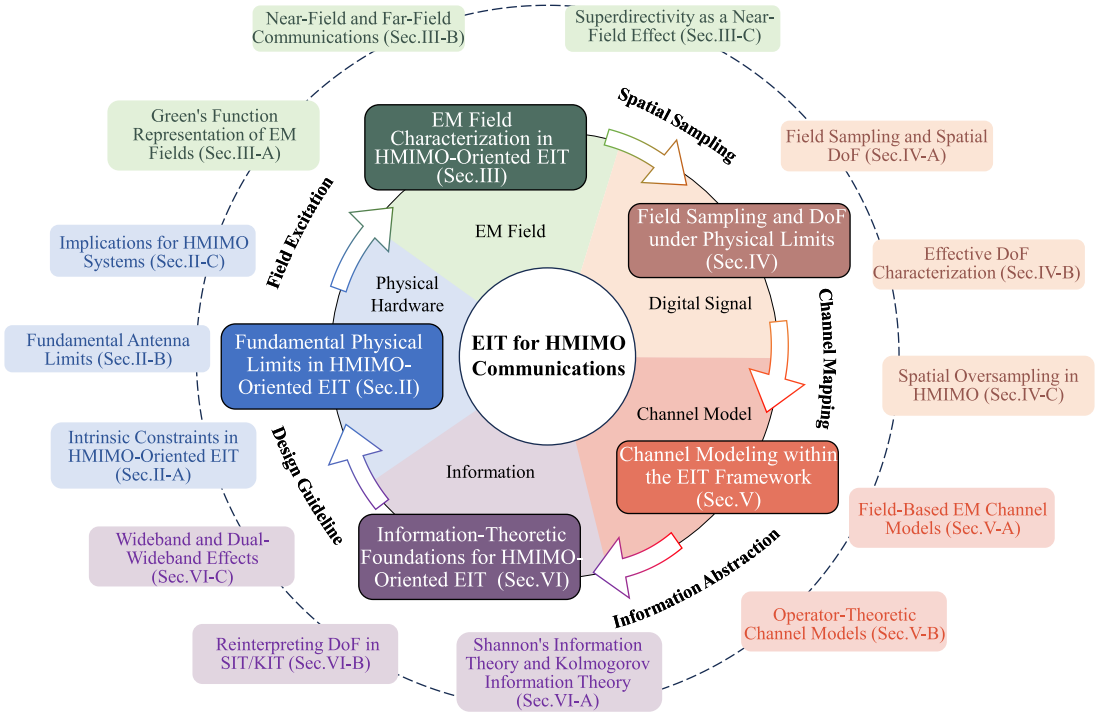

Fig. 2. Main structure of the article.

II. FUNDAMENTAL PHYSICAL LIMITS IN HMIMO-ORIENTED EIT

This section investigates the intrinsic physical constraints imposed by antenna design on HMIMO systems, which fundamentally affect key performance metrics such as array gain and bandwidth. The objective is to elucidate the relationship between the physical antenna configuration and the overall system performance. To this end, we discuss the fundamental challenges and inherent physical limitations associated with the maximum directivity gain G, the minimum quality factor Q (approximately inversely proportional to bandwidth), and the achievable gain G_r, which is influenced by the energy efficiency η_{ee}. The implications of these physical limits for HMIMO systems are also examined. For ease of understanding, the overall structure of this section is illustrated in Fig. 3.

A. Intrinsic Physical Constraints

Compact HMIMO systems, while offering unprecedented spatial resolution and array gain, face intrinsic constraints that directly impact their performance in wireless communications. These limitations arise from fundamental antenna properties, which in turn restrict achievable system metrics such as bandwidth, spectral efficiency, and capacity.

1) High-Q Resonance and Narrowband Sensitivity: The excitation of higher-order radiation modes in dense HMIMO arrays often increases the quality factor Q, thereby leading to narrowband operation [50]. Since Q is inversely proportional to the fractional bandwidth B_n, we have $B_n = \frac{f_h - f_l}{f_0} = \frac{1}{Q}$, where f_h and f_l are the upper and lower cutoff frequencies of the operational band, and $f_0 = (f_h + f_l)/2$ is the resonant frequency. The cutoff frequencies are typically defined at the

Authorized licensed use limited to: Zhejiang University. Downloaded on May 24,2026 at 03:23:22 UTC from IEEE Xplore. Restrictions apply.

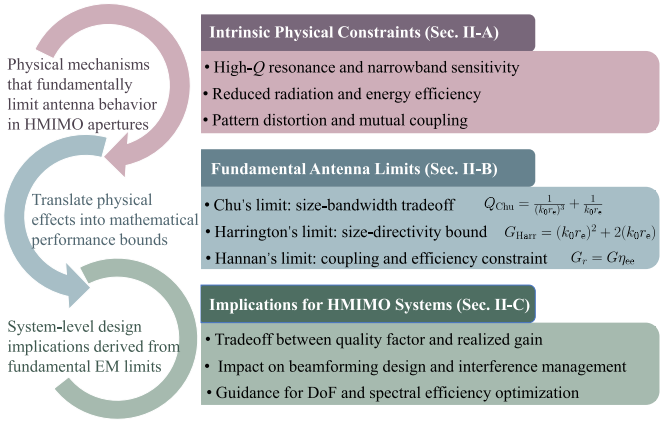

Fig. 3. Framework of Sec. II.

half-power points of the radiated spectrum. A high Q thus implies a narrow operational bandwidth, which limits the available frequency-domain DoF and constrains the achievable data rate. This sensitivity is particularly detrimental for broadband HMIMO applications such as mmWave and THz communications, where wideband signaling is essential for high throughput (see Sec. VI-C for further discussion).

2) Reduced Radiation and Energy Efficiency: The energy efficiency η_{ee} characterizes how effectively an antenna converts the input electrical power into radiated EM power. It is defined as the ratio between the radiated gain and the total (theoretical) directivity gain, i.e., $G_r = \eta_{\mathrm{ee}} G$, where G denotes the ideal directivity gain determined by the radiation pattern, and G_r represents the achievable (realized) gain after accounting for ohmic losses and mutual coupling. In practical wireless systems, a reduced η_{ee} directly lowers the received SNR and link reliability. For example, decreasing the element spacing below $\lambda/2$ may theoretically increase array directivity G but simultaneously degrade efficiency due to stronger near-field coupling and resistive losses. In massive HMIMO deployments, this tradeoff between gain and efficiency fundamentally affects both energy consumption and coverage—two key metrics for sustainable and power-efficient 6G operation.

3) Pattern Distortion and Mutual Coupling: Ideally, HMIMO arrays should maintain stable and uniform radiation patterns to ensure consistent beamforming and multi-user separation [51]. However, dense element packing introduces strong mutual coupling, which distorts radiation patterns across the array [52]. Central elements may retain predictable patterns, but edge elements often exhibit pronounced deviations. Such pattern non-uniformity undermines spatial multiplexing performance and increases inter-user interference, ultimately limiting the multi-user capacity achievable by HMIMO systems.

The above intrinsic challenges highlight how fundamental antenna constraints—namely the directivity gain G and quality factor Q—directly map onto wireless system performance metrics including capacity, bandwidth efficiency, link reliability, and energy consumption. These interrelations underscore the necessity of revisiting classical antenna limits (Chu's, Harrington's, and Hannan's limit) in the HMIMO context, as elaborated in the following subsection.

B. Fundamental Antenna Limits

The maximum directivity gain G and the minimum quality factor Q are fundamentally bounded by Chu's and Harrington's limits. These classic limits provide physical insights into the tradeoff among bandwidth, resonance, and directivity. Furthermore, the achievable array gain, when mutual coupling among elements is considered, is constrained by Hannan's limit. Together, these limits delineate the physical operating regime of HMIMO arrays within the EIT framework.

1) Chu's Limit [53]: Chu's limit describes the fundamental tradeoff between antenna size and bandwidth. It establishes the minimum achievable quality factor Q for an antenna enclosed within a sphere of radius r_e as

$$Q_{\mathrm{Chu}} = \frac{1}{(k_0 r_{\mathrm{e}})^3} + \frac{1}{k_0 r_{\mathrm{e}}}. \tag{1}$$

This relation shows that smaller antennas ($k_0 r_e \ll 1$) inherently exhibit larger Q and thus narrower bandwidth. Although the same spherical-mode framework can be extended to estimate directivity scaling with $(k_0 r_e)^2$, Chu's analysis primarily focused on the Q–bandwidth limitation. For compact HMIMO arrays, this limit implies that further miniaturization enhances spatial resolution but restricts the available bandwidth and overall data throughput, posing challenges for wideband 6G communications.

2) Harrington's Limit [54]: Harrington extended Chu's spherical-mode framework by including both transverse electric (TE) and transverse magnetic (TM) modes—two orthogonal vector spherical components that together describe the radiated field—leading to the following upper bound on antenna directivity:

$$G_{\mathrm{Harr}} = (k_0 r_{\mathrm{e}})^2 + 2(k_0 r_{\mathrm{e}}). \tag{2}$$

The corresponding minimum quality factor is given by [55]:

$$Q_{\mathrm{Harr}} = \frac{1}{2(k_0 r_{\mathrm{e}})^3} + \frac{1}{k_0 r_{\mathrm{e}}}. \tag{3}$$

Later studies [56] showed that compact arrays may exceed G_{Harr} through optimal excitation, implying the possibility of superdirectivity. Although superdirective HMIMO arrays can theoretically enhance spatial DoF, they suffer from high Q and low radiation efficiency, which limits their practical applicability in wireless communication systems. This behavior reflects the fundamental energy trade-off in antenna theory: achieving higher directivity (larger G) requires exciting higher-order spherical modes that store more reactive energy, thereby increasing the quality factor Q and reducing the effective bandwidth.

Fig. 4 compares the maximum directivity gain G among Chu's limit, Harrington's limit, and near-field spherical modes [55]. The near-field region allows higher effective directivity than predicted by these far-field limits, highlighting the potential advantages of near-field HMIMO operation. Fig. 5 compares the quality factors corresponding to Chu's limit,

Authorized licensed use limited to: Zhejiang University. Downloaded on May 24,2026 at 03:23:22 UTC from IEEE Xplore. Restrictions apply.

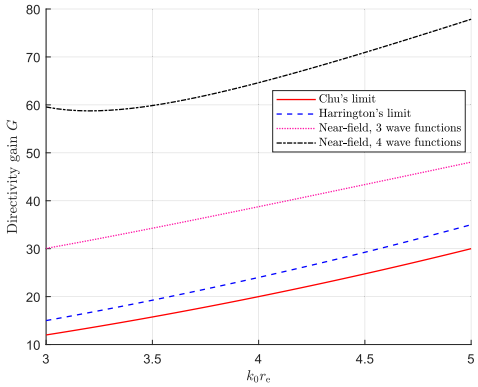

Fig. 4. Maximum directivity gain G for Chu's approach, Harrington's approach, and different number of spherical modes in near-field in [55].

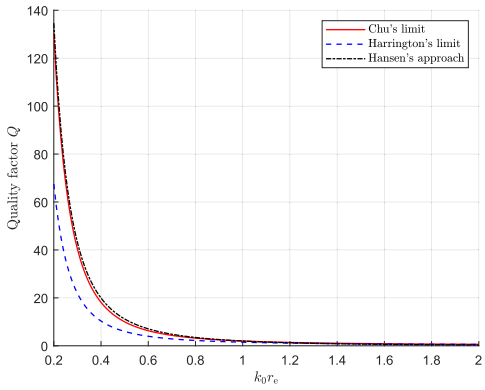

Fig. 5. Minimum quality factor Q for Chu's limit, Harrington's limit, and Hansen's approach.

Harrington's limit, and Hansen's approach [57]. Chu's limit represents the theoretical minimum Q, corresponding to the narrowest possible bandwidth and serving as the lower bound for practical antenna designs.

Overall, Chu's limit applies to electrically small antennas and specifies the minimum achievable Q (or maximum bandwidth) for a given size, whereas Harrington's limit extends this framework to include both TE and TM modes and provides an upper bound on directivity for antennas of arbitrary electrical size. Together, they describe complementary bounds that jointly characterize the trade-off between size, bandwidth, and gain in practical antenna and HMIMO array designs.

3) Hannan's Limit [58]: Hannan's limit characterizes the impact of mutual coupling on array performance. It establishes how the ideal directivity gain G deteriorates into a more realistic realized gain G_r when element interactions and efficiency losses are taken into account. Specifically, the maximum directivity gain for an antenna element is

$$G(\theta) = \frac{4\pi A_{\text{eff}}}{\lambda^2}\cos\theta, \tag{4}$$

where A_{eff} is the effective aperture area for each antenna element in the array, and θ is the scanning angle.

The expression in (4) originates from aperture antenna theory and represents the maximum theoretical directivity achievable when each element radiates independently and losslessly. In practice, however, when the total array aperture is fixed, increasing the number of elements—while seemingly capable of improving the overall gain—inevitably reduces the inter-element spacing. This leads to stronger mutual coupling and a decrease in each element's effective radiating area, thereby offsetting the potential gain improvement and resulting in the achievable gain given by [58]

$$G_r(\theta) = \frac{4\pi A_{\text{eff}}}{\lambda^2}\cos\theta \cdot \eta_{\text{ee}}, \tag{5}$$

which accounts for the embedded radiation efficiency η_{ee}.

The theoretical radiation efficiency, i.e., maximum element efficiency for a dense array (e.g., HMIMO systems), is [59]

$$[\eta_{\text{ee}}]_{\max} = \frac{G_r}{G} = \frac{\pi A_{\text{eff}}}{\lambda^2}, \tag{6}$$

with ideal directivity limit $G = 4$ for an electrically small antenna above a perfectly reflecting ground plane.

The practical radiation efficiency can be further quantified using two equivalent formulations, based on the active reflection coefficient and the scattering matrix, respectively.

- Using the active reflection coefficient $R(\alpha,\beta)$[1] over the excitation phasings (α,β), η_{ee} is obtained as [58]:

$$\eta_{\text{ee}} = 1 - \frac{1}{\pi^2}\int_{\alpha=0}^{\pi}\int_{\beta=0}^{\pi}|R(\alpha,\beta)|^2 \mathrm{d}\alpha\mathrm{d}\beta, \tag{7}$$

  where $\eta_{\text{ee}} = \pi/4$ for the ideal element in an infinite array with spacing $\lambda/2$.
- Resorting to the scattering matrix S-parameter, η_{ee} can be approximated by [60]

$$\eta_{\text{ee}} = 1 - \sum |S_{ij}|^2. \tag{8}$$

Both $R(\alpha,\beta)$ in (7) and S_{ij} in (8) reflect mutual coupling, $R(\alpha,\beta)$ is reflection coefficient that dependent on excitation phasings (α,β) while S_{ij} is the S-parameter between inactive i-th and active j-th ports. Typically, (7) is an upper limit to (8), and (8) is much more applicable than (7) to the medium-size to small arrays [59].

Two types of gains should be distinguished: (i) the maximum directivity gain $G(\theta)$ in (4), representing the ideal case for an infinite array, and (ii) the realized gain $G_r(\theta)$ in (5), which accounts for ohmic dissipation and impedance mismatch. The realized gain is more relevant to practical communication performance, as it reflects real-world losses and inter-element interactions.

However, the degradation in realized gain is undesirable, motivating efforts to overcome Hannan's limit. Recent work [61] experimentally demonstrated that 3D array configurations exhibit higher radiation efficiency than their 2D counterparts due to the enlarged effective aperture, effectively relaxing Hannan's limit. This finding suggests that novel 3D or non-coplanar array structures could further enhance achievable gain and potentially break the traditional performance constraints in wireless communications.

[1]Here, $R(\alpha,\beta)$ denotes the reflection coefficient corresponding to a particular pair of excitation phasings (α,β), which represent the relative phase excitations applied across the array to steer the beam in different directions. The integral in (7) therefore averages the reflected power over all possible excitation states.

Authorized licensed use limited to: Zhejiang University. Downloaded on May 24,2026 at 03:23:22 UTC from IEEE Xplore. Restrictions apply.

C. Implications for HMIMO Systems

Clearly, the maximum directivity G and the minimum quality factor Q cannot be achieved simultaneously. A higher G typically implies a narrower beamwidth and, consequently, a higher Q. Therefore, HMIMO system design must jointly consider these two quantities rather than optimizing either one in isolation.

To illustrate this tradeoff, consider a sectored antenna gain model for both the base station (BS) and user sides [62]:

$$G_b(\theta_b) = \begin{cases} G_b^{\max}, & |\theta_b| \le B_b, \\ G_b^{\min}, & \text{otherwise}, \end{cases} G_u(\theta_u)$$
$$= \begin{cases} G_u^{\max}, & |\theta_u| \le B_u, \\ G_u^{\min}, & \text{otherwise}. \end{cases}$$

Here, B_b and B_u denote the beamwidths of the BS and user antenna arrays, respectively.

The alignment of the main lobes (θ_b, θ_u) directly determines the overall array gain $G_b^{\max} G_u^{\max}$ in line-of-sight (LoS) conditions. In practice, beam patterns may exhibit sidelobes and non-uniform gain distributions. Such sidelobes cause interference leakage from undesired directions in multi-user scenarios, making sidelobe suppression crucial for interference mitigation.

The beamwidth B is approximately inversely proportional to the quality factor Q, i.e., $B \propto 1/Q$. This relationship follows from the classical definition of Q as the ratio between stored and radiated energy—where higher Q corresponds to stronger field confinement and thus a narrower angular radiation profile. Consequently, the tradeoff between G and Q also represents the tradeoff between beam sharpness and operational bandwidth. System designers should therefore identify an optimal Q that balances spatial focusing and spectral efficiency, depending on antenna geometry and aperture size [63].

While increasing beam gain improves received SNR, it can also exacerbate inter-user interference if sidelobes are not well controlled. Nevertheless, directional HMIMO arrays inherently enhance SNR and reduce interference leakage due to their narrow main lobes, enabling energy-efficient operation across sub-6 GHz and sub-THz regimes.

Finally, the advantages of forming multiple narrow beams in HMIMO can be understood through the concept of spatial DoF, i.e., each distinct beam corresponds to an independent field distribution at the receiver. Thus, by generating multiple non-overlapping beams, HMIMO arrays effectively increase the number of distinguishable field patterns and hence the achievable information throughput.

III. EM Field Characterization in HMIMO-Oriented EIT

Following the discussion of physical constraints, this section shifts the focus from antenna-level limitations to field-level representations. Within the EIT framework, the HMIMO channel is interpreted as a continuous EM transformation between the transmitter and receiver. Accordingly, we revisit the fundamentals of EM wave theory and analyze far-field and near-field interactions to reveal their impacts on propagation wavefront, polarization diversity, capacity and spatial DoF in emerging wireless systems.

A. Green's Function Representation of EM Fields

In the EIT framework, the EM field acts as the continuous carrier of information. Its behavior is governed by Maxwell's equations, which describe the coupling between electric sources and radiated fields [64], [65]. From these equations, the dyadic Green's function can be derived as a fundamental operator that linearly maps the source current distribution on the HMIMO aperture to the resulting field distribution at the receiver domain. In this sense, the Green's function serves as the deterministic "channel kernel" linking excitation and observation within EIT.

1) Deterministic Dyadic Green's Function: For a point current source $\mathbf{J} = \bar{\mathbf{I}}\delta(\cdot)$, the dyadic identity tensor $\bar{\mathbf{I}} = \hat{x}\hat{x} + \hat{y}\hat{y} + \hat{z}\hat{z}$ serves as the unit dyad, which maps any vector onto itself and preserves its direction. The radiated electric field $\mathbf{E}(\mathbf{r})$ in free space can be expressed as

$$\mathbf{E}(\mathbf{r}) = -j\omega\mu \int_S \overline{\mathbf{G}}_0(\mathbf{r}, \mathbf{r}') \cdot \mathbf{J}(\mathbf{r}')\, \mathrm{d}s', \tag{9}$$

where S denotes the HMIMO aperture. Here $\overline{\mathbf{G}}_0(\mathbf{r}, \mathbf{r}')$ is the dyadic Green's function of free space, defined as

$$\overline{\mathbf{G}}_0(\mathbf{r}, \mathbf{r}') = \left[\bar{\mathbf{I}} + \frac{\nabla\nabla}{k_0^2}\right] g(\mathbf{r}, \mathbf{r}'), \tag{10}$$

where $k_0 = 2\pi/\lambda$ is the free-space wavenumber and $g(\mathbf{r}, \mathbf{r}')$ is the scalar Green's function given by

$$g(\mathbf{r}, \mathbf{r}') = \frac{e^{-jk_0|\mathbf{r}-\mathbf{r}'|}}{4\pi|\mathbf{r}-\mathbf{r}'|}. \tag{11}$$

In a homogeneous medium, $\overline{\mathbf{G}}_0$ depends only on the spatial distance $|\mathbf{r} - \mathbf{r}'|$ [66]. Equation (9) thus describes a deterministic linear mapping from current excitation to radiated field—an EM analogue of the channel impulse response in communications.

2) Stochastic Dyadic Green's Function: In realistic wireless environments, multiple reflections, scattering, and diffraction processes introduce randomness into the field distribution. According to the central limit theorem, the superposition of numerous randomly phased multipath components leads to a complex Gaussian field [29], motivating the stochastic dyadic Green's function representation that incorporates environmental randomness through eigenvalue and eigenfunction perturbations [67], [68]:

$$\overline{\mathbf{G}}_{\mathrm{S}}(\mathbf{r}, \mathbf{r}') = \sum_i \frac{\mathbf{\Psi}_i(\mathbf{r}, k_i) \otimes \mathbf{\Psi}_i(\mathbf{r}', k_i)}{k^2 - k_i^2 - jk^2/\tilde{Q}}, \tag{12}$$

where $\tilde{Q}$ denotes the cavity quality factor, k_i and $\mathbf{\Psi}_i$ represent the i-th perturbed wavenumber and orthogonal vectorial eigenfunctions of the random medium. Each eigenfunction can be approximated as a random superposition of plane-wave components:

$$\Psi_i^{\theta}(\mathbf{r}, k_i) \simeq \sum_n a_n \cos\psi_n \cos(k_i \hat{\mathbf{e}}_n \cdot \mathbf{r} + \beta_n), \tag{13}$$

$$\Psi_i^{\phi}(\mathbf{r}, k_i) \simeq \sum_n a_n \sin\psi_n \cos(k_i \hat{\mathbf{e}}_n \cdot \mathbf{r} + \beta_n), \tag{14}$$

Authorized licensed use limited to: Zhejiang University. Downloaded on May 24,2026 at 03:23:22 UTC from IEEE Xplore. Restrictions apply.

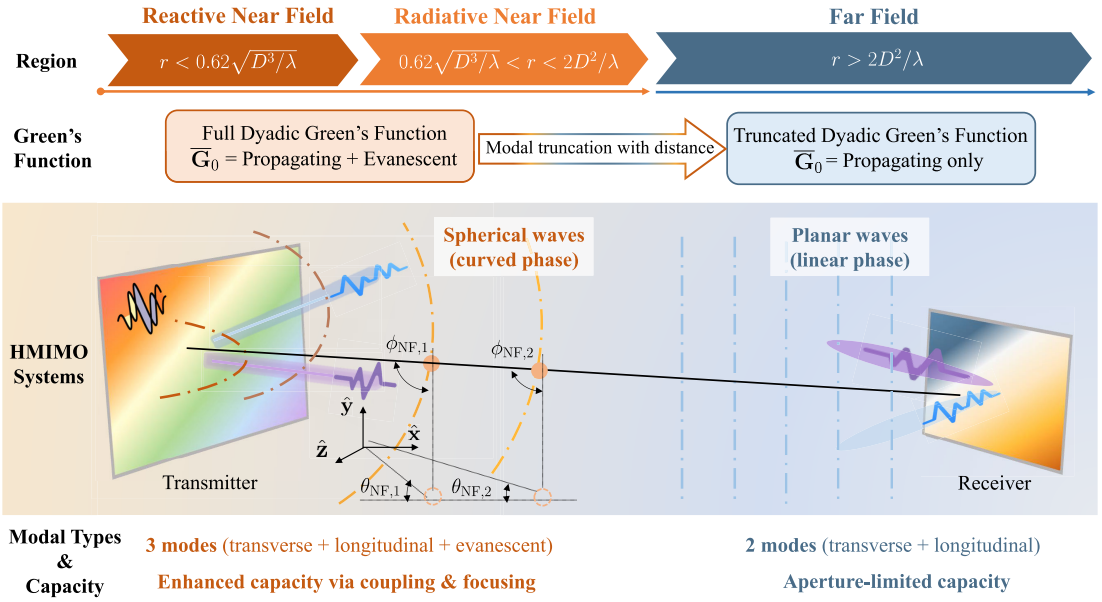

Fig. 6. Near-field and far-field communications.

where a_n, $\hat{\mathbf{e}}_n$, and β_n denote the amplitude, direction, and random phase of each plane-wave component, respectively. This stochastic formulation naturally decomposes the total field into a coherent (deterministic) component and an incoherent (diffuse) component [69], [70], thereby bridging deterministic EM wave theory and statistical channel modeling under the HMIMO-oriented EIT framework.

B. Near-Field and Far-Field Communications

The spatial behavior of the EM field described by the dyadic Green's function in (9) naturally reveals the continuous transition between near-field and far-field communications. Specifically, the kernel $\overline{\mathbf{G}}_0(\mathbf{r}, \mathbf{r}')$ encapsulates both the propagating and evanescent components of the field through its spherical-wave expansion. At large observation distances, the slowly decaying propagating modes dominate, forming the far-field regime; whereas at shorter distances, the rapidly decaying evanescent modes become significant, leading to the near-field regime characterized by strong spatial coupling between the transmitter and receiver. This gradual modal transition establishes the EM foundation of distance-dependent field behavior.

To quantify these regions, the general boundary between the near-field and far-field is given by the Rayleigh distance, $r = 2D^2/\lambda$, where D denotes the antenna aperture. For completeness, the near-field zone is further divided into a reactive near field ($r < 0.62\sqrt{D^3/\lambda}$) and a radiating near field ($0.62\sqrt{D^3/\lambda} < r < 2D^2/\lambda$), depending on whether the reactive or radiative components dominate. Beyond this range ($r > 2D^2/\lambda$), the field enters the far-field (Fraunhofer) region, where only propagating plane-wave components remain. These boundaries are consistent with the modal interpretation derived from the dyadic Green's function.

As illustrated in Fig. 6, the far-field region exists beyond the Rayleigh distance, while the near field lies within it. These two regimes can be interpreted as distinct truncations of the dyadic Green's function: i) retaining only the propagating terms of $\overline{\mathbf{G}}_0$ yields a plane-wave model for the far field, and ii) including both propagating and evanescent components recovers the full spherical-wave model for the near field. Hence, the following key differences emerge from the same EM formulation.

- **Propagation Wavefront:** In the far-field regime, where the phase variation across the aperture is approximately linear, the radiated field can be represented as a superposition of plane waves sharing identical azimuth and elevation angles $(\theta_{\mathrm{FF}}, \phi_{\mathrm{FF}})$. Conversely, in the near-field region, the curvature of the spherical wavefront introduces distance-dependent phase variations across antenna elements, leading to element-specific angular parameters $(\theta_{\mathrm{NF},i}, \phi_{\mathrm{NF},i})$ [71]. This curvature stems directly from the second-order derivative term $\nabla\nabla g(\mathbf{r}, \mathbf{r}')$ in $\overline{\mathbf{G}}_0$, which accounts for coupling and phase nonuniformity.
- **Polarization Diversity:** The dyadic operator $\overline{\mathbf{I}} + \nabla\nabla/k_0^2$ also determines the polarization structure of the field. In the near field, where both transverse and longitudinal field components are significant, three orthogonal polarization modes exist. In contrast, in the far field, the longitudinal component vanishes asymptotically, and only two transverse polarizations remain. This reduction corresponds to a rank deficiency in $\overline{\mathbf{G}}_0$ as $|\mathbf{r} - \mathbf{r}'| \to \infty$, explaining the loss of one polarization DoF in the far-field limit.
- **Capacity and Spatial DoF:** From an EM perspective, each orthogonal eigenmode of $\overline{\mathbf{G}}_0$ represents an independent spatial channel. In the near field, the presence of evanescent and longitudinal modes enriches the eigenspectrum, leading to additional DoF compared to the far field [72], [73]. Although the power of higher-order modes decays rapidly with distance, their contribution becomes non-negligible within the Rayleigh zone, where coupling between antenna elements and spatial

Authorized licensed use limited to: Zhejiang University. Downloaded on May 24,2026 at 03:23:22 UTC from IEEE Xplore. Restrictions apply.

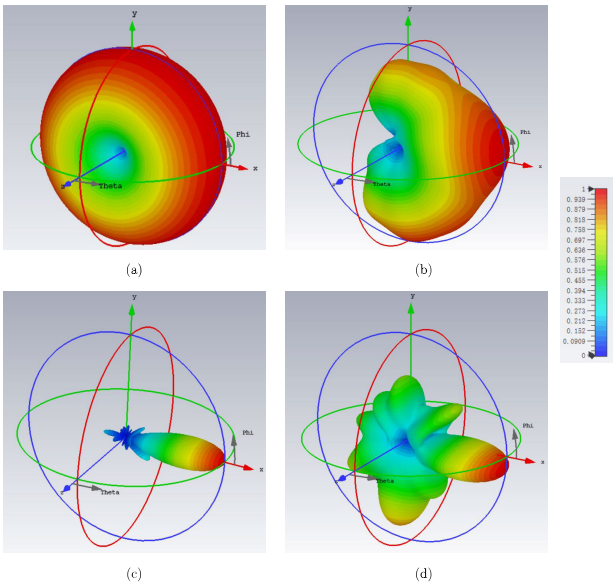

Fig. 7. Radiation pattern for (a) an isolated antenna; (b) individual antenna in HMIMO with spacing 0.3λ; (c) HMIMO with spacing 0.3λ; (d) HMIMO with spacing 0.4λ.

non-stationarity prevail. These extra DoF correspond to additional eigenchannels that jointly enhance the achievable capacity and enable more efficient spatial focusing.

In summary, the near- and far-field distinctions are not merely geometric but directly emerge from the modal composition of the dyadic Green's function. The near field activates additional spatial eigenmodes (including evanescent ones), expanding the effective rank of $\overline{\mathbf{G}}_0$ and thus increasing the information-carrying capability of HMIMO systems under the EIT framework. This physically grounded interpretation bridges the EM channel modeling in Sec. V and information-theoretic analysis developed in Sec. VI.

C. Superdirectivity as a Near-Field Effect

Building upon the physical constraints of gain and quality factor discussed in Sec. II, this part focuses on the EM mechanisms that enable superdirectivity in HMIMO systems. The phenomenon originates from the excitation of higher-order modes in the near-field region, where mutual coupling and reactive energy storage reshape the field distribution and expand the available modal DoF. As illustrated in Fig. 7 (CST simulation), the radiation pattern of an isolated element [Fig. 7(a)] becomes distorted under strong coupling [Fig. 7(b)], but can be shaped into a superdirective pattern through optimized excitation coefficients and inter-element spacing [Fig. 7(c)–(d)].

In near-field HMIMO architectures, such superdirective behavior enhances spatial focusing and increases the number of excited field modes, offering additional DoF for information transfer. The reactive near-field energy—often neglected in conventional designs—can jointly carry and modulate information in the electric and magnetic domains. Consequently, the classical Rayleigh limit (e.g., $\lambda/2$) for spatial resolution may be surpassed, provided that advanced receivers are employed to handle the resulting non-orthogonal field structures.

From a system perspective, superdirective arrays can achieve beamforming gains scaling as N^2 in ideal case, in contrast to the conventional N scaling of far-field MIMO with $\lambda/2$ spacing. The excitation coefficients (beamforming weights) can be designed using the coupling matrix [74], enabling constructive interference among tightly coupled elements. Experimental results in [75] demonstrate that superdirective arrays can achieve up to ninefold higher spectral efficiency than conventional MIMO systems, even with a smaller aperture.

However, superdirectivity comes at a cost. The high concentration of reactive energy reduces overall radiation efficiency, leading to lower realized gain G_r despite increased directivity G. Moreover, precise excitation control is required to achieve the desired current distributions, posing challenges for dense planar or patch-based arrays. These tradeoffs are closely tied to the G–Q relationship: achieving extreme directivity inevitably incurs penalties in bandwidth and efficiency.

In summary, superdirectivity represents an intriguing HMIMO regime that may surpass classical physical limits by exploiting near-field reactive energy. Realizing this regime in practice, however, demands precise array calibration, robust excitation control, and possibly new sensing and detection architectures capable of harnessing the additional reactive DoF rather than treating them as parasitic effects. The excitation of higher-order reactive modes fundamentally increases the number of distinguishable field patterns, setting the stage for a quantitative discussion of field sampling and spatial DoF the next section.

IV. Field Sampling and DoF Under Physical Limits

The EM field is inherently continuous and carries rich spatial information, yet only a limited portion of this information can be captured or transmitted in practice. Within the framework of EIT, this section examines how continuous fields can be discretized through field sampling, and how the number of distinguishable spatial modes (or DoF) is constrained by physical limits such as aperture size and wavelength. This formulation establishes the theoretical basis for efficient antenna deployment and offers practical insights into how compact HMIMO arrays can exploit spatial oversampling to enhance overall system performance. For ease of understanding, the overall structure of this section is illustrated in Fig. 8.

A. Field Sampling and Spatial DoF

Field sampling refers to representing a continuous EM field through a finite set of discrete spatial measurements. From this viewpoint, the array of antenna elements acts as a sampling mechanism: by probing the field at specific locations in space, it becomes possible to approximate and, under suitable conditions, reconstruct the underlying field distribution. This sampling process naturally raises the question of how densely these measurements must be taken without losing information.

In classical communications, this requirement is captured by the Nyquist sampling theorem, which provides the fundamental criterion for interference-free signal reconstruction.

Authorized licensed use limited to: Zhejiang University. Downloaded on May 24,2026 at 03:23:22 UTC from IEEE Xplore. Restrictions apply.

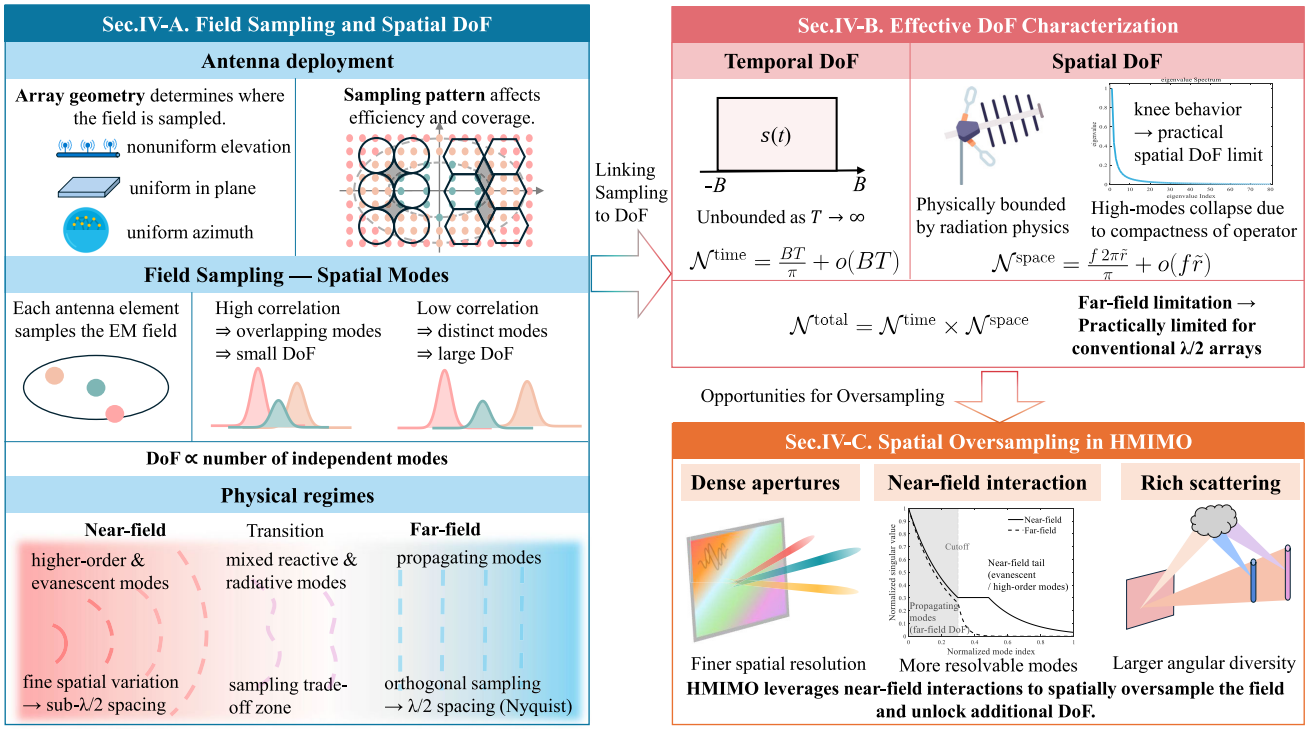

Fig. 8. Framework of Sec. IV.

It ensures that a continuous-time waveform can be perfectly recovered when it is sampled at a rate at least twice its highest frequency component, thereby preventing spectral aliasing in the frequency domain [42], [76]. Analogously, in the spatial domain, an EM field can be regarded as a continuous function of space, and sampling it at sufficiently fine spatial intervals enables the reconstruction of the field distribution. The spatial counterpart of the Nyquist rate specifies that antenna elements should be spaced approximately $\lambda/2$ apart to avoid spatial aliasing. Interestingly, this spacing is also widely adopted in practical antenna design and in theoretical analysis in wireless communications, as it provides a good trade-off between reducing mutual coupling and maintaining alias-free spatial sampling.

In practice, spatial sampling is implemented by placing discrete antenna elements in space, and the array geometry determines how this sampling is carried out. For example, linear arrays sample nonuniformly over elevation, circular arrays provide uniform sampling over azimuth but not elevation, whereas spherical arrays achieve uniform sampling in both azimuth and elevation directions [77], [78]. Three-dimensional apertures further extend the sampling domain, yielding a larger spatial coverage compared with one- and two-dimensional configurations [79]. Beyond the array geometry itself, the choice of sampling pattern also affects efficiency: for instance, hexagonal sampling offers denser spatial coverage with less redundancy than rectangular sampling [80].

Beyond the geometric arrangement of antenna elements, spatial sampling can also be interpreted from an informational perspective. Each antenna element provides a local observation of the surrounding EM field. When these observations are distinguishable, i.e., correspond to linearly independent field components, they contribute to independent spatial signaling dimensions at the transceiver. The number of such independent dimensions is commonly interpreted as the spatial DoF of the channel [80], which serves as an information-theoretic measure of how many independent spatial modes can be resolved, transmitted, or received within a given aperture.

The attainable DoF, however, is ultimately constrained by the physical characteristics of the EM field and the propagation environment. In the far field, the distinguishable modes are primarily associated with plane-wave directions, for which an inter-element spacing of approximately $\lambda/2$ is typically sufficient to capture all propagating components without aliasing. In the near field, by contrast, the EM field also contains higher-order and rapidly decaying components that carry additional spatial structure. Capturing these localized, non-propagating modes often requires sampling at a density higher than the conventional $\lambda/2$ spacing. This contrast between the far-field and near-field regimes therefore highlights the importance of characterizing not only the theoretical DoF but also the practically attainable DoF, which depends on the spatial sampling density and the underlying field structure. This aspect is further examined in the following subsection.

B. Effective DoF Characterization

There are two common viewpoints for quantifying the DoF in EM and wireless systems. The first viewpoint estimates the number of physically supported modes — i.e., a theoretical spatial DoF — by examining the singular-value spectrum of the underlying channel or field operator and retaining only the dominant modes [26], [81], [82]. This interpretation is widely

Authorized licensed use limited to: Zhejiang University. Downloaded on May 24,2026 at 03:23:22 UTC from IEEE Xplore. Restrictions apply.

adopted and admits a geometric picture in terms of packing distinguishable field patterns or signaling waveforms in a high-dimensional space (see Sec. VI-B). The second viewpoint is more operational: it counts the number of modes that remain energetically active in the capacity-achieving solution, which can be characterized through the nonzero optimal source L^2 norms [28]. In other words, it measures how many modes are actually used under optimal excitation, rather than how many modes exist in principle.

In practice, these two viewpoints need not agree exactly. When the singular values decay smoothly without a clear cutoff, as often occurs in near-field regimes, it becomes ambiguous to define a hard truncation threshold on "dominant" modes, and the operational definition may better reflect the practically usable DoF. Nevertheless, for analytical clarity and for connection to classical sampling and array design, in this subsection we adopt the spectral (truncation-based) viewpoint. Under this viewpoint, the DoF is determined by the concentration of the operator's eigenvalue (or singular value) spectrum: only a finite number of modes carry significant energy, while the remaining modes become negligible. This leads naturally to Landau's and Slepian's analysis of time- and band-limited function spaces [83], [84], and subsequent refinements such as [85], which show that only a finite set of eigenmodes carries most of the energy within a constrained time–bandwidth or space–wavenumber region. We now make this characterization explicit for a physically realizable EM source.

Scatterers and Spatial DoF Gain

It is a well-accepted fact that additional spatial gain is achieved in the scattering environment. However, the justification for such a spatial gain is controversial.

Specifically, Janaswamy [86] proved that the presence of scatterers will slow the decaying rate of higher mode powers in the near field (e.g, decays algebraically), and the slowing is much more dramatic if the scatterers are closer to the observation circle, which further increases the DoF. Therefore, Janaswamy argues that much of the benefit of increased NDoF comes from scatterers. However, Franceschetti et al. present a contradictory conclusion in [87] that the information gain is purely a near-field effect that is independent of scatterers, especially for large-sized communication systems.

In fact, the conclusions drawn from [86] and [87] are valid in their respective regimes, as investigated in [78] from the following aspects:

1) If a finite aperture is considered (as assumed in [86]) in a rich scattering environment, the scatterers would subtend all possible angles on the observation plane. Therefore, the additional DoF is induced and attributed to backscattering effects, which supports the conclusion in [86].
2) On the other hand, if an infinite aperture (as assumed in [87]) is considered in LOS-only propagation, the aperture also subtends all possible angles on the observation plane. Therefore, the scatterers cannot increase angular extent beyond LOS-only propagation, and the additional DoF gain is a purely near-field gain, which assures the conclusion in [87].
3) However, if the aperture is finite in the LOS-only case, the angles subtended by the aperture are much less than that in an infinite aperture, and the additional DoF is also decreased [78].

Consequently, based on the relationship between the subtended angles and DoF, the contradictory conclusions drawn from [86] and [87] are explainable.

Considering a circular radiating source of physical radius r that encloses both the emitter and relevant scatterers [85], and define the normalized radius $\tilde{r} = r/c$, where c is the speed of light. A cut-set boundary separates the source and receiver, so that the radiated field in the receive region is fully determined by the field on this boundary [85]. The field is observed over a finite time interval $t \in [-T/2, T/2]$ and within a frequency band $f \in [-B, B]$. Spatially, it is observed over the angular interval $\phi \in [-\pi, \pi]$ and occupies a wavenumber band $w \in [-W, W]$, where the spatial (angular) wavenumber support scales as $w = f\tilde{r} + o(f\tilde{r})$ as $f\tilde{r} \to \infty$. Equivalently, the wavenumber bandwidth[2] satisfies $W \approx 2\pi B\,\tilde{r}$.

Following the variation of Landau's eigenvalue theorem in [85], we consider the limiting cases in which either the observation time or the bandwidth becomes arbitrarily large, corresponding to the time-limited and band-limited formulations, respectively. The resulting DoFs are given by

$$\mathcal{N}^{\mathrm{BL}} = \frac{BT}{\pi} \cdot \frac{2\pi\tilde{r}B}{2\pi} + o(\tilde{r}T), \quad \tilde{r}, T \to \infty, \tag{15}$$

and

$$\mathcal{N}^{\mathrm{TL}} = \frac{BT}{\pi} \cdot \frac{2\pi\tilde{r}B}{2\pi} + o(\tilde{r}B), \quad B \to \infty. \tag{16}$$

These expressions are asymptotically equivalent and reveal that the total DoF scales with both the time–bandwidth product BT and the effective spatial bandwidth $2\pi\tilde{r}B$. Equivalently, the total DoF can be interpreted as the product of a temporal DoF term and a spatial DoF term.

The temporal DoF corresponds to a one-dimensional signal that is either time-limited to $t \in [-T/2, T/2]$ or band-limited to $f \in [-B, B]$, and is given by

$$\mathcal{N}^{\mathrm{time}} = \frac{BT}{\pi} + o(BT), \quad BT \to \infty. \tag{17}$$

This scaling shows that temporal DoF can be increased by either enlarging the bandwidth B or extending the observation time T. In principle, it becomes unbounded as $T \to \infty$.

The spatial DoF represents the number of distinguishable angular field modes that can be radiated at frequency f and observed on the circular boundary $\phi \in [-\pi, \pi]$, which is

$$\mathcal{N}^{\mathrm{space}} = \frac{f\,2\pi\tilde{r}}{\pi} + o(f\tilde{r}), \quad f\tilde{r} \to \infty. \tag{18}$$

Hence, spatial DoF may be increased either by enlarging the effective aperture size r (increasing $\tilde{r}$) or by exploiting multipath scattering in the environment, which effectively enriches the number of resolvable angular modes. The former is often constrained by size and cost, whereas the latter is more practical in HMIMO systems. A more detailed discussion of

[2]A circular source of radius r cannot excite arbitrarily high angular modes: the highest significant angular mode index scales on the order of $kr = 2\pi f\tilde{r}$, and evaluating this at the edge of the band $f = B$ yields $W \approx 2\pi B\tilde{r}$.

Authorized licensed use limited to: Zhejiang University. Downloaded on May 24,2026 at 03:23:22 UTC from IEEE Xplore. Restrictions apply.

scatterer-induced spatial DoF gain is provided in the text box "Scatterers and Spatial DoF Gain".

The total DoF in (15) and (16) highlights that both temporal and spatial resources jointly determine the overall system capability. However, in practical EM systems, these DoF components cannot scale independently due to inherent physical and design constraints. For instance, increasing the bandwidth B generally requires lowering the minimum quality factor Q, which reduces the achievable directivity gain G (see Sec. II). A lower directivity weakens the separability of spatial modes, thereby diminishing the effective spatial DoF even as the temporal DoF increases. Hence, extending bandwidth alone does not necessarily lead to a higher total or practically attainable DoF; the temporal and spatial contributions must be considered jointly.

From a theoretical viewpoint, the temporal DoF can grow without bound as the observation time increases, whereas the spatial DoF is fundamentally limited by the compactness of the channel operator $\mathcal{A}$. Its singular values exhibit a "knee" behavior—decaying slowly in the near-field regime but rapidly in the far-field—thus imposing a deterministic upper bound on the number of resolvable spatial modes [26]. This classical limitation motivates the exploration of HMIMO systems, where dense spatial sampling and near-field interactions offer new opportunities for exploiting additional spatial DoF beyond conventional array designs.

C. Spatial Oversampling in HMIMO

The previous subsection showed that the spatial DoF is ultimately limited. In a conventional far-field array, once the antenna elements are spaced at approximately $\lambda/2$, the dominant propagating modes are already captured. Adding more elements with even denser spacing mainly re-samples the same modes, so the effective spatial DoF saturates. However, HMIMO changes this operating regime. By densely populating a large, essentially continuous aperture, HMIMO not only samples far-field plane-wave modes but also senses and shapes finer spatial structure such as near-field wavefront curvature, evanescent/reactive components, and other high-order modes that decay rapidly with distance and are invisible to a conventional critically sampled array.

This motivates the use of spatial oversampling, which places elements with sub-$\lambda/2$ spacing to deliberately capture these fast-varying field components. Such dense sampling can increase the effective spatial DoF available to the transceiver, but it is not free—closely spaced elements become strongly correlated, analogous to inter-symbol interference (ISI) in time-domain signaling. This implies that HMIMO benefits not only from orthogonal spatial channels, but also from managing useful non-orthogonality in space.

This "spatial oversampling" should not be confused with faster-than-Nyquist (FTN) signaling. FTN, following Mazo [88], increases the symbol rate beyond the Nyquist limit in the time domain by allowing controlled nonorthogonality between pulses, while keeping the minimum Euclidean distance between symbols essentially unchanged [89]. By contrast, spatial oversampling in HMIMO is a physical sampling strategy: it is dictated by aperture size, wavelength, and near-field coupling, rather than by excess temporal bandwidth.

Therefore, the organizing principle behind FTN, namely the idea of deliberately allowing interference and resolving it through advanced receiver processing, is conceptually useful. Similarly, HMIMO can adopt this philosophy in the spatial domain. Instead of enforcing strictly orthogonal beams and $\lambda/2$ element spacing, the array can tolerate controlled inter-element correlation (spatial "ISI") and recover information through joint processing across elements. In this view, correlation is regarded as a resource rather than merely a penalty.

However, directly porting FTN-style techniques to the spatial domain is nontrivial. Even in the temporal case, FTN requires more complex detection and compensation mechanisms: carefully designed non-sinc pulses or precoding to reduce interference, as well as additional signal processing to handle increased peak-to-average power ratio, such as clipping, constellation extension, and selected mapping. These techniques reduce the receiver burden but introduce their own impairments. This suggests that while FTN provides an analogy for HMIMO, it should be regarded as an inspiration for future spatial transceiver designs rather than as an off-the-shelf solution.

V. Channel Modeling Within the EIT Framework

Within the EIT framework, the communication channel is represented as an EM operator that maps the transmitted field to the received field through the Green's function of the environment. This section introduces several EM-compliant channel models that progressively capture the physical and statistical nature of propagation. Specifically, the field-based EM channel models—including the plane-wave spectral expansion model, the dyadic Green's function (DGF) model, and the stochastic Green's function (SGF) model—are presented. Finally, the continuous aperture representation extends these models to the continuous spatial domain, linking physical field operators to the HMIMO channel characteristics.

Division of Green's Functions in Far-/Near-Fields

Through Weyl's decomposition, the scalar free-space Green's function in (11) which satisfies the inhomogeneous Helmholtz equation with a δ-function source is expanded by a series of plane waves, i.e. [90], [91],

$$\frac{e^{-jk_0 r}}{r} = \frac{-jk_0}{2\pi} \int\int_{-\infty}^{\infty} \frac{1}{k_z} \exp[-jk_0(k_x x + k_y y + k_z|z|)] dk_x dk_y, \quad (19)$$

where $k_z = \sqrt{1 - k_x^2 - k_y^2}$ for $\mathcal{D}(k) = \{(k_x, k_y) \mid k_x^2 + k_y^2 \leqslant 1\}$, $k_z = -j\sqrt{k_x^2 + k_y^2 - 1}$ for $\bar{\mathcal{D}}(k) = \{(k_x, k_y) \mid k_x^2 + k_y^2 > 1\}$.

Therefore, the scalar function $g(\mathbf{r})$ is the sum of integrals in two parts, i.e., $G(\mathbf{r}) = G_H(\mathbf{r}) + G_E(\mathbf{r})$ [90].

The homogeneous part $G_H(\mathbf{r})$ contains all propagating plane waves in the far-field zone, which is given by

$$G_H(\mathbf{r}) = \frac{-jk_0}{2\pi} \int\int_{\mathcal{D}(k)} \frac{1}{k_z} \exp[-jk_0(k_x x + k_y y$$

Authorized licensed use limited to: Zhejiang University. Downloaded on May 24,2026 at 03:23:22 UTC from IEEE Xplore. Restrictions apply.

$$+ k_z|z|)]dk_x dk_y \overset{(a)}{=} -jk_0 \int_0^1 \times \exp[-j\alpha(z)v] J_0\left[\beta(x,y)\sqrt{1-v^2}\right] dv, \quad (20)$$

where (a) makes use of polar coordinates, J_0 is the Bessel function of the first kind and order zero, the coordinate-dependent parameters $\alpha(z) = k_0|z|$ and $\beta(x,y) = k_0\sqrt{x^2+y^2}$, and v is radial integration variable [90].

Similarly, the evanescent part $G_E(\mathbf{r})$ contains all the exponentially decaying plane waves in the near-field zone, i.e.,

$$G_E(\mathbf{r}) = \frac{-jk_0}{2\pi} \int\int_{\bar{\mathcal{D}}} \frac{1}{k_z} \exp[-jk_0(k_x x + k_y y + k_z|z|)]dk_x dk_y = k_0 \int_0^\infty \times \exp[-\alpha(z)v] J_0\left[\beta(x,y)\sqrt{v^2+1}\right] dv. \quad (21)$$

A. Field-Based EM Channel Models

The current distribution $\mathbf{J}$ imposed by the transmit point source excites an EM wave $\mathbf{E}$ under the transfer function $\overline{\mathbf{G}}_0$ (or $\overline{\mathbf{G}}_S$ in the presence of scattering). The concept of wireless channels, widely used in communications, has not been well established yet from the EM perspective. To gain a comprehensive understanding of EM channels, we interpret the EM channel as a continuous vector wave field excited by an impulse response. As a consequence, the (stochastic) dyadic Green's functions can be considered as the EM-domain wireless channel (denoted by $\mathbf{H}$) for systems with continuous apertures. In this context, the channel inherently satisfies the vector Helmholtz equation, i.e.,

$$\nabla \times \nabla \times \mathbf{H} - k_0^2 \mathbf{H} = \mathbf{0}, \quad (22)$$

where $\mathbf{H}$ can be alternatively chosen as one of its representations in different domains. For example, the channel can be in a space-time representation, $\mathbf{H} = \mathbf{H}(\mathbf{r}, t)$ or in a wavenumber-time representation, $\mathbf{H} = \mathbf{H}(\mathbf{k}, t)$, with the following Fourier transformation relation

$$\mathbf{H}(\mathbf{r}, t) = \frac{1}{(2\pi)^3} \int \mathbf{H}(\mathbf{k}, t) e^{j\mathbf{k}\cdot\mathbf{r}} d\mathbf{k}, \quad (23)$$

where $\mathbf{k} = [k_x, k_y, k_z]^T$ is the wavevector, and the integration is performed over region $\mathcal{D} = \{k_x^2 + k_y^2 + k_z^2 = k_0^2\}$. Furthermore, the integral region can be divided into region $k_x^2 + k_y^2 \le k^2$ for supporting propagating waves existing in far-field, and region $k_x^2 + k_y^2 > k^2$ including evanescent waves in the near-field region. See the text box "Division of Green's Functions in Far-/Near-Fields" for details of the scalar channel scenario. Such a division in the wavenumber domain is consistent with the communication region divided in the space domain.

1) Deterministic Channel Models: Deterministic models describe the propagation channel through explicit EM formulations, without assuming statistical randomness. Here, two representative deterministic models—the Fourier plane-wave expansion model and the dyadic Green's function model—are introduced to interpret field propagation in rich-scattering and LoS environments, respectively.

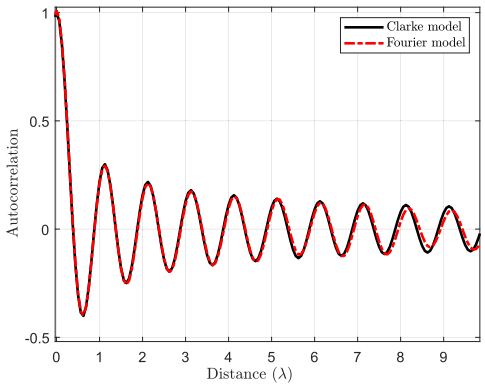

Fig. 9. Comparison between Fourier plane wave expansion model and traditional Clarke model in terms of the autocorrelation function vs. distance between two antennas [101] (source codes from [102]).

a) Fourier plane-wave expansion model: The Fourier plane-wave expansion model provides a physically consistent representation of the channel in the wavenumber (angular) domain. It represents the received field as a superposition of plane waves emitted from different directions, thereby approximating the multipath propagation process in a deterministic but spatially rich manner.

Specifically, when the homogeneous part $G_H(\mathbf{r})$ of the Green's function dominates within a finite circular wavenumber region $\mathcal{D}$, the field can be expressed by a finite number of plane-wave components [80]. The spatial channel response between the transmit point $\mathbf{s}$ and the receive point $\mathbf{r}$ is [92]:

$$h(\mathbf{r}, \mathbf{s}) = \frac{1}{(2\pi)^2} \iiint\int_{\mathcal{D}(k)\times\mathcal{D}(\kappa)} a_r(k_x, k_y, \mathbf{r})\, H_a(k_x, k_y, \kappa_x, \kappa_y) \times a_s(\kappa_x, \kappa_y, \mathbf{s})\, d\ k_x dk_y d\kappa_x d\kappa_y, \quad (24)$$

where a_r and a_s denote the receive and source response functions, respectively, and H_a is the angular transfer function that characterizes how each transmit direction (κ_x, κ_y) contributes to the received direction (k_x, k_y).

When the environment is isotropic, $H_a(k_x, k_y, \kappa_x, \kappa_y)$ can be factorized into separable transmit and receive terms, leading to an approximately uncorrelated angular-domain channel. This decomposition enables low-complexity beamspace processing and sparse channel estimation in far-field scenarios. In the near-field regime, however, the coupling between angular components becomes significant, and the Fourier representation captures these interactions more accurately than classical uncorrelated scattering models.

As shown in Fig. 9, the spatial autocorrelation function (i.e., $R(d) \triangleq \frac{\mathbb{E}\{h(\mathbf{r})h^*(\mathbf{r}+\mathbf{d})\}}{\mathbb{E}\{|h(\mathbf{r})|^2\}}$, where $\mathbf{d} = [d, 0, 0]^T$) of the Fourier model closely matches that of the classical Clarke model [93] for small antenna separations, validating its effectiveness in rich-scattering environments.

Limitations: The Fourier plane-wave expansion model assumes that scatterers can be represented by regular surfaces (planar, cylindrical, or spherical), where the field decomposition into harmonic components is tractable. For irregular or complex scattering environments, numerical methods such

Authorized licensed use limited to: Zhejiang University. Downloaded on May 24,2026 at 03:23:22 UTC from IEEE Xplore. Restrictions apply.

as the method of moments are preferred, where the dyadic Green's function is employed to compute the induced currents and coupling effects. Therefore, the Fourier-based representation is best suited for analytically tractable deterministic scenarios, while Green's function formulations offer a more general framework, as discussed next.

b) Dyadic green's function model: To capture the complex EM interactions in near-field communications, various modeling approaches have been proposed [32], [94], [95], [96], [97], [98], [99]. A commonly used approach is the spherical wave expansion, which represents the channel as a superposition of spherical harmonics whose coefficients are often modeled as Gaussian random variables. This framework allows modeling both far-field and near-field components by controlling the ratio between the two regions [95]. However, spherical wave models mainly serve as mathematical interpolation tools without explicit physical interpretation of polarization or current distribution, which may limit their accuracy and result in underestimated system capacity.

To overcome these limitations, the DGF is introduced for physically rigorous channel modeling. Unlike the spherical-wave approximation, the DGF formulation directly stems from Maxwell's equations and inherently accounts for polarization, mutual coupling, and field continuity across arbitrary surfaces. Its effectiveness has been demonstrated in [32], where the DGF-based formulation accurately captures the variation of spatial DoF between near-field and far-field regions. Subsequent studies [35], [96] further extended this model to HMIMO systems in LoS near-field communications, offering a unified EM interpretation that encompasses power gain, polarization diversity, and spatial correlation.

Specifically, by partitioning the HMIMO aperture into N_s small patches, the total electric field at an observation point can be computed as the superposition of radiations from all sub-elements, i.e.,

$$\mathbf{E}(\mathbf{r}) = \sum_{n=1}^{N_s} \int\int dx_0' dy_0' \left[\bar{\mathbf{I}} + \frac{\nabla\nabla}{k_0^2}\right] \frac{e^{-jk_0 r_n}}{4\pi r_n} \cdot \mathbf{J}(\mathbf{r}_n'), \quad (25)$$

where $\mathbf{J}(\mathbf{r}_n')$ denotes the current at the n-th source patch, and r_n is the distance from the patch to the observation point. In this formulation, each transmit patch contributes to the total received field via its DGF kernel. For compact HMIMO arrays, the receiver may lie in the near-field region with respect to the array aperture, yet still be in the far-field region relative to each individual element—an important observation enabling hybrid near–far-field modeling. This framework has been further extended to arbitrarily shaped transmitting and receiving surfaces [100].

The performance of the DGF model has been verified through correlation comparisons with the traditional Clarke model, as shown in Fig. 10. It can be observed that the two models exhibit consistent correlation behavior across different antenna spacings, validating the EM-compliant formulation.

Limitations: Although the DGF model provides a physically complete description of polarization and field interactions, its computational complexity remains high, particularly in environments with numerous random scatterers. For multi-path or strongly scattering channels, directly solving the DGF becomes impractical. Therefore, in such cases, stochastic Green's function models are adopted to capture random scattering effects in a computationally efficient manner, as discussed in the next subsection.

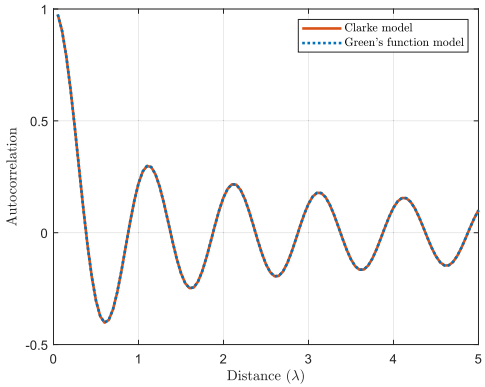

Fig. 10. Comparison between Green's function model and traditional Clarke model in terms of the autocorrelation function vs. distance between two antennas [32].

2) Stochastic Channel Models: To effectively capture the randomness of scatterers in practical wireless environments, SGF models have been developed as statistical extensions of deterministic EM formulations. Unlike the Fourier plane-wave expansion, which is limited to regular scattering geometries, or the DGF, which is computationally intensive for random multipath environments, the SGF approach models the Green's function itself as a random field with statistically defined properties. This enables a physically consistent yet probabilistic description of multi-path propagation within the EIT framework.

The SGF formulation originates from the random wave model and random matrix theory, which treats the complex EM field as a spatially correlated Gaussian process [68]. The eigenfunction $\mathbf{\Psi}_i(\mathbf{r}, k_i)$ of the stochastic Helmholtz equation at position $\mathbf{r}$ can be expressed as

$$\mathbf{\Psi}_i(\mathbf{r}, k_i) \simeq w_i^x \hat{\mathbf{x}} + w_i^y \hat{\mathbf{y}} + w_i^z \hat{\mathbf{z}}, \quad (26)$$

where w_i^x, w_i^y, and w_i^z are correlated Gaussian random variables defined by the statistical superposition of plane waves

$$\begin{aligned} w_i^x &\simeq \lim_{N\to\infty} \sum_{n=1}^{N} [a_n (-\cos\psi_n \sin\phi_n \\ &\quad - \sin\psi_n \cos\phi_n \cos\theta_n) \cos(k_i \hat{\mathbf{e}}_n \cdot \mathbf{r} + \beta_n)], \\ w_i^y &\simeq \lim_{N\to\infty} \sum_{n=1}^{N} [a_n (\cos\psi_n \cos\phi_n \\ &\quad - \sin\psi_n \sin\phi_n \cos\theta_n) \cos(k_i \hat{\mathbf{e}}_n \cdot \mathbf{r} + \beta_n)], \\ w_i^z &\simeq \lim_{N\to\infty} \sum_{n=1}^{N} [a_n \sin\psi_n \sin\theta_n \cos(k_i \hat{\mathbf{e}}_n \cdot \mathbf{r} + \beta_n)], \end{aligned} \quad (27)$$

where a_n is the n-th plane wave amplitude satisfying $\langle a_m a_n \rangle = \frac{2}{NV}\delta_{mn}$, V is the cavity volume, and ψ_n, ϕ_n, and θ_n denote polarization, azimuth, and elevation angles, respectively. This representation allows the local field components to be modeled as Gaussian-distributed random variables,

Authorized licensed use limited to: Zhejiang University. Downloaded on May 24,2026 at 03:23:22 UTC from IEEE Xplore. Restrictions apply.

TABLE II
FIELD-BASED CHANNEL MODELS

Channel Modeling Methods	Related Works	Applicable Scenarios	Limitations
Fourier plane wave expansion model	[92], [101]	Approximately represent the spatial NLoS path with less wavenumber-domain samples at low cost.	Difficult to handle irregular scatterers.
Dyadic Green's function model	[32], [35], [96]	Exactly describe both near-field and far-field LoS scenarios using dyadic Green's functions.	Computationally prohibitive in NLoS modeling.
Stochastic Green's function model	[67], [68], [104], [105]	Statistically depict the general scattering environment using random wave model and random matrix theory.	High complexity; difficult to obtain statistics of model parameters.

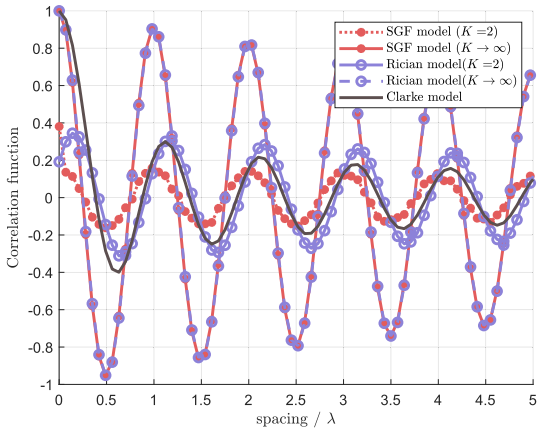

Fig. 11. Comparison between SGF model and traditional Rician and Clarke model in terms of the autocorrelation function vs. distance between two antennas [103].

consistent with the statistical isotropy of complex scattering environments.

The resulting SGF defines the channel transfer function as a random operator whose eigenvalues and eigenvectors follow probabilistic distributions determined by the ensemble of scattering realizations. Motivated by this formulation, the work in [103] proposed a universal EM-compliant channel model for HMIMO systems, where the SGF is used to statistically represent the superposition of a large number of plane waves. This approach allows the derivation of the mean and variance of the field amplitudes for different polarization states and spatial locations, thereby linking EM wave statistics with channel characteristics such as capacity, correlation, and spatial DoF.

The EM-compliant behavior of the SGF model across different antenna spacings has been verified through correlation comparisons with the traditional Rician model and Clarke model, as shown in Fig. 11.

Limitations: Despite its strong physical foundation, the SGF model faces challenges when applied to open wireless environments. The theory was originally developed for closed or quasi-closed cavities with known geometric parameters (volume, boundary conditions, etc.) [68]. Extending it to general propagation scenarios—where boundary information is incomplete or continuously varying—remains an open research problem. Future work is expected to generalize the SGF concept by incorporating environmental priors (e.g., from ray tracing or environmental maps) into the EM framework.

A comparison among different channel modeling approaches, including their applicable scenarios and limitations, is summarized in Table II.

B. Operator-Theoretic Channel Models

While the previous stochastic models statistically describe field randomness induced by complex scattering, they are still grounded in discrete array representations. To unveil the fundamental physical limits of wireless communications within the EIT framework, it is necessary to move beyond discrete antennas and analyze the propagation process in the continuous aperture domain. Such a formulation enables an intrinsic evaluation of the system performance that is independent of the number of antenna elements or their spacing, thus providing a more fundamental EM perspective of HMIMO systems.

Unlike the discrete channel matrices in conventional models, the continuous aperture channel is characterized by square-integrable functions and Hilbert–Schmidt operators. Specifically, both the channel operator $k(\mathbf{r},\mathbf{s})$ and input signal $f(\mathbf{s})$ are square-integrable functions: $f : \mathbb{R}^d \to \mathbb{C}$ satisfying $\int |k(\mathbf{r},\mathbf{s})|^2 < \infty$ and $\int |f(\mathbf{s})|^2 < \infty$. Defining the Hilbert–Schmidt operator $\mathcal{H} : L^2(\mathbb{R}^d) \to L^2(\mathbb{R}^d)$, the input-output mapping is given by

$$\mathcal{Y} = (\mathcal{H}f)(\mathbf{s}) = \int k(\mathbf{r},\mathbf{s}) f(\mathbf{s}) d\mathbf{s}. \tag{28}$$

The detailed relationships between integral operators in continuous domains and their discrete matrix counterparts can be found in [106, Table I].

The orthonormal eigenfunctions of the transmitter space $\mathcal{S}_T$ and receiver space $\mathcal{S}_R$ can effectively characterize the continuous channel. Specifically, the input signal $f(\mathbf{s})$ is represented by a set of orthonormal basis functions $\{\phi_n(\mathbf{s})\}_{n\in\mathbb{N}}$ and the radiated field is expressed using eigenfunction set $\{\psi_n(\mathbf{r})\}_{n\in\mathbb{N}}$. A real sequence $\{\xi_n\}_{n\in\mathbb{N}}$ (i.e., the singular values of the channel operator), converging to zero, satisfies the following relation:

$$\mathcal{H}f = \sum_{n=1}^{\infty} \xi_n \langle f, \phi_n(\mathbf{s}) \rangle \psi_n(\mathbf{r}), \tag{29}$$

Authorized licensed use limited to: Zhejiang University. Downloaded on May 24,2026 at 03:23:22 UTC from IEEE Xplore. Restrictions apply.

where the Hilbert-Schmidt kernel $k(\mathbf{r},\mathbf{s}) = \sum_{n=1}^{\infty} \xi_n \phi_n \psi_n^*$ is connected to Green's function $\overline{\mathbf{G}}_0(\mathbf{r},\mathbf{s})$ [43].

Consequently, the eigenfunctions of the transmitter and receiver apertures form the natural basis for continuous channel modeling.

1) Optimal Eigenfunctions: In the point-to-point transmission, the receiver basis function $\psi(\mathbf{r})$ and transmitter basis function $\phi(\mathbf{s})$ are connected via the integral of the Green's function $\overline{\mathbf{G}}_0(\mathbf{r},\mathbf{s})$ over the transmit space $\mathcal{S}_T$, i.e., $\psi(\mathbf{r}) = \int_{\mathcal{S}_T} \overline{\mathbf{G}}_0(\mathbf{r},\mathbf{s})\phi(\mathbf{s})d\mathbf{s}$. Therefore, the optimal eigenfunctions can be derived by solving a coupled eigenfunction problem given by [107], [108, Eq.(12)-(15)]

$$\begin{aligned} \xi_n^2 \phi_n(\mathbf{s}) &= \int_{\mathcal{S}_T} K_T(\mathbf{s},\mathbf{s}')\,\phi_n(\mathbf{s}')\,d\mathbf{s}', \\ \xi_n^2 \psi_n(\mathbf{r}) &= \int_{\mathcal{S}_R} K_R(\mathbf{r},\mathbf{r}')\,\psi_n(\mathbf{r}')\,d\mathbf{r}', \end{aligned} \tag{30}$$

where

$$\begin{aligned} K_T(\mathbf{s}',\mathbf{s}) &= \int_{\mathcal{S}_R} \overline{\mathbf{G}}_0^*(\mathbf{r},\mathbf{s}) \cdot \overline{\mathbf{G}}_0(\mathbf{r},\mathbf{s}')\,d\mathbf{r} \\ K_R(\mathbf{r},\mathbf{r}') &= \int_{\mathcal{S}_T} \overline{\mathbf{G}}_0(\mathbf{r},\mathbf{s}) \cdot \overline{\mathbf{G}}_0^*(\mathbf{r}',\mathbf{s})\,d\mathbf{s}. \end{aligned} \tag{31}$$

However, finding these optimal eigenfunctions analytically is generally intractable. Typically, one has to resort to EM simulations, e.g., Galerkin's method. Yet, these numerical methods become impractical for large antenna arrays due to unacceptable computational complexity. Consequently, it is recommended to approximate the continuous channel using discretization methods or alternative approximate eigenfunctions.

2) Integral Over Discretized Spaces: Discretizing the transmitter and receiver spaces is an effective solution to address eigenfunction problems. This transforms the continuous eigenfunction problem into an SVD problem with a finite and discretized dimension [107].

Specifically, for each discretized patch, the integral counterpart of channel matrix $\mathbf{H}$ is $\mathcal{H} : L^2(\mathbb{R}^2) \to L^2(\mathbb{R}^2)$, i.e.,

$$(\mathcal{H}x)(\mathbf{r}) = \int h(\mathbf{r},\mathbf{t})x(\mathbf{s})\mathrm{d}\mathbf{s}, \tag{32}$$

where $h(\mathbf{r},\mathbf{t})$ is the coupling coefficient between the transmitter and receiver surfaces, and $h(\mathbf{r}_m,\mathbf{t}_n) = \mathbf{H}_{mn}$ in the discrete case.

With the aid of Riemann sum approximation, the singular value relation between the continuous and discretized representations is given by [106]

$$\sigma_k(\mathbf{H}) \approx \sqrt{\frac{N_t N_r}{\mathcal{A}_t \mathcal{A}_r}}\sigma_k(\mathcal{H}), \tag{33}$$

where $\mathcal{A}_t$ and $\mathcal{A}_r$ are the Lebesgue measure of transmitter and receiver on $\mathbb{R}^2$.

However, this method relies on the small-aperture approximation and assumes an unblocked direct path between the transmitter and receiver. Therefore, extending this approach to large apertures imposes significant challenges on the computational costs.

3) Other Choices of Approximate Eigenfunctions: In addition to direct discretization, several analytical families of approximate eigenfunctions can be employed to represent the continuous aperture channel. Representative examples include the prolate spheroidal wave functions, Fourier modes [109], and focusing functions that allow the transmitter aperture to concentrate energy efficiently toward specific spatial regions [108]. The choice of basis functions depends on the communication scenario, boundary conditions, and aperture geometry.

By exploiting the compactness of the aperture set and the integrability of the kernel function, one can further characterize the asymptotic behavior of singular values, which directly determines the number of effective DoF of the channel. The detailed DoF analysis and its implications for EIT are presented in Sec. VI.

Limitations: The continuous channel modeling relies heavily on the selection of eigenfunctions. However, solving for the optimal eigenfunctions by addressing the coupled eigenfunction problems is often intractable. Even though discretizing the transmitter and receiver into small segments and treating them as piecewise constant basis functions can reduce the computational burden to some extent, this approach becomes impractical for large apertures. Therefore, it is crucial to design feasible and near-optimal approximate eigenfunctions that balance computational efficiency with communication performance requirements.

VI. Information-Theoretic Foundations for HMIMO-Oriented EIT

This section revisits information measures from probabilistic and deterministic viewpoints to formulate an EIT basis tailored to HMIMO systems. Specifically, we examine SIT and KIT as two complementary frameworks. SIT models the statistical relationship between inputs and outputs in a probabilistic setting [15], whereas KIT adopts a deterministic, functional-analytic perspective to quantify information carried by continuous fields [25]. Although rooted in different mathematical formulations, both converge to a common physical insight within the EIT framework—namely, that the number of resolvable modes (DoF) is determined by the available aperture, bandwidth, and propagation environment.

A. Shannon's Information Theory and Kolmogorov Information Theory

To establish a comprehensive understanding of information measures in EIT, it is instructive to revisit two foundational paradigms—SIT and KIT—which respectively adopt probabilistic and deterministic formulations. These two theories are not mutually exclusive but rather complementary, offering distinct yet consistent perspectives on information representation, as shown in Fig. 12.

1) Shannon's Information Theory (SIT): In SIT, the *Shannon capacity* quantifies the maximum reliable information rate under a probabilistic communication model [15]. A useful visualization is a sphere-packing picture in an N_{SIT}-dimensional signal space (Fig. 12): each codeword corresponds to a point specified by N_{SIT} orthonormal coordinates,

Authorized licensed use limited to: Zhejiang University. Downloaded on May 24,2026 at 03:23:22 UTC from IEEE Xplore. Restrictions apply.

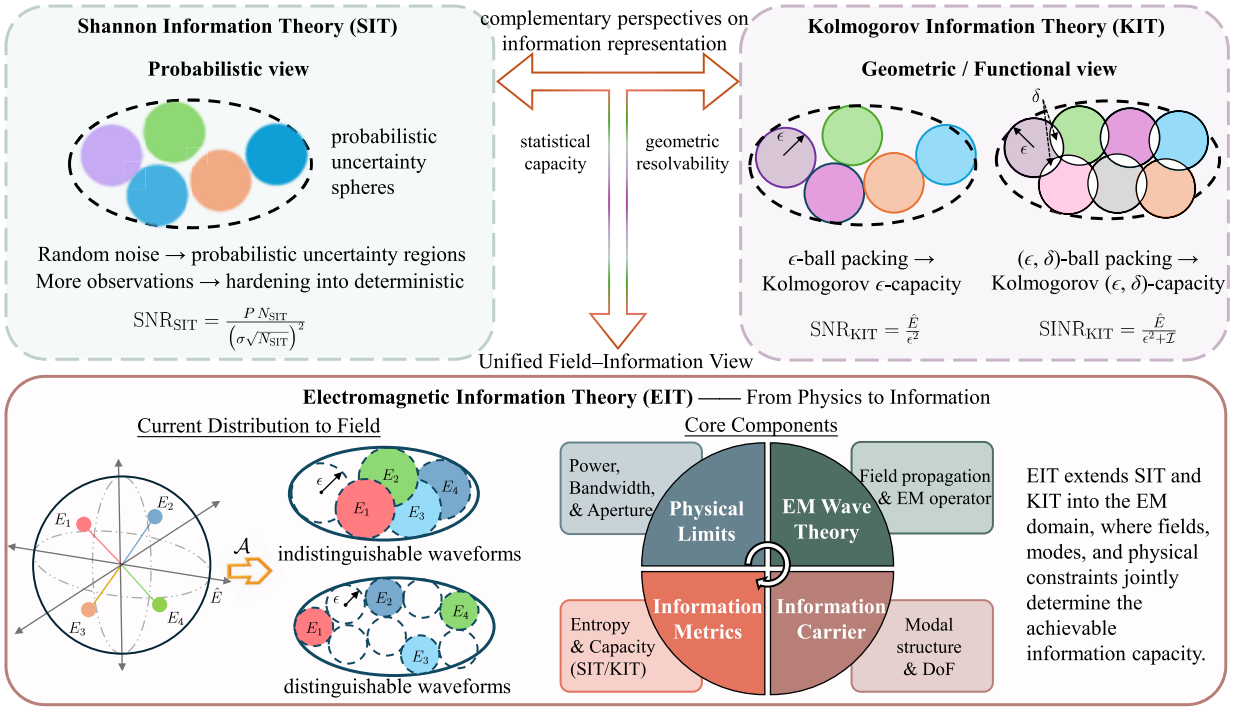

Fig. 12. Conceptual relationship among SIT, KIT, and EIT.

and additive noise induces an uncertainty region around each point. As the observation resources grow ($T \to \infty$ and/or $B \to \infty$), these "soft" regions concentrate toward "hard" spheres. Counting the number of non-overlapping spheres (denoted here by N_{SIT}) provides a geometric intuition: the available distinguishable codewords scale as $\log_2 N_{\mathrm{SIT}}$. This packing count is a conceptual proxy for distinguishability; the actual Shannon capacity further depends on SNR and bandwidth. For reference, the SNR in this picture is [81]

$$\mathrm{SNR}_{\mathrm{SIT}} = \frac{P\, N_{\mathrm{SIT}}}{\left(\sigma\sqrt{N_{\mathrm{SIT}}}\right)^2}, \tag{34}$$

where P is the transmitted power per symbol and $\sigma\sqrt{N_{\mathrm{SIT}}}$ is the uncertainty radius induced by noise. While SIT rigorously optimizes over input distributions, it typically requires full probabilistic specification, which obscures the contribution of individual spatial/temporal modes in complex EM scenes. This motivates a complementary deterministic view via KIT.

2) Kolmogorov's Information Theory (KIT): KIT assesses information deterministically by counting the number of distinguishable signals under a fixed resolution ϵ. An infinite-dimensional function class is approximated by a finite-dimensional subspace whose ϵ-balls do not overlap, leading to the *Kolmogorov ϵ-capacity* [25], [81]. This is again a packing problem (Fig. 12), but with "hard" balls of radius ϵ that represent instrument/implementation uncertainties (e.g., antenna tolerances, measurement errors). If the signal energy is bounded by $\hat{E}$ (e.g., for band-limited fields), a natural SNR proxy is

$$\mathrm{SNR}_{\mathrm{KIT}} = \frac{\hat{E}}{\epsilon^2}, \tag{35}$$

and the count of non-overlapping ϵ-balls, N_{KIT}, yields the information measure $\log_2 N_{\mathrm{KIT}}$. To connect SIT and KIT, a relaxed (ϵ, δ)-capacity allows controlled overlap between ϵ-balls with relative overlap δ, representing a target decoding error [81] (Fig. 12). In multi-user scenarios, interference enlarges the uncertainty radius to $\epsilon_{\mathrm{MU}} = \epsilon + \sqrt{\mathcal{I}}$ (with interference energy $\mathcal{I}$), and

$$\mathrm{SINR}_{\mathrm{KIT}} = \frac{\hat{E}}{\epsilon^2 + \mathcal{I}}. \tag{36}$$

Remarks: SIT and KIT apply to both time and space due to space–time symmetry. Geometrically, both quantify information by counting how many non-overlapping balls fit in the image ellipsoid of an operator—the ϵ-packing problem. The difference lies in uncertainty modeling: SIT begins with probabilistic "soft" uncertainty that hardens with large observations (law of large numbers), whereas KIT assumes a fixed resolution ϵ from the outset. The two views are thus complementary: SIT emphasizes statistical capacity; KIT emphasizes geometric resolvability—both essential to EIT.

3) Visualization via Compact Operators: Within EIT, the input–output relationship between the source current distribution and the radiated EM field can be formulated as an operator mapping $\mathcal{A} : X \to Y$, as also visualized in Fig. 12. The operator $\mathcal{A}$ is analytic and compact, and it depends on the propagation environment and boundary conditions. It can be expressed through the Hilbert–Schmidt decomposition [26]:

$$Ax = \sum_{k=1}^{\infty} \sigma_k \langle x, v_k \rangle u_k, \tag{37}$$

where $\{v_k\}$ and $\{u_k\}$ denote the right and left singular functions, σ_k are the singular values, and $\langle \cdot, \cdot \rangle$ is the inner product

Authorized licensed use limited to: Zhejiang University. Downloaded on May 24,2026 at 03:23:22 UTC from IEEE Xplore. Restrictions apply.

in $L^2(X)$. Due to the compactness of $\mathcal{A}$, the singular values decay monotonically as $\sigma_1 \geq \sigma_2 \geq \ldots$ and $\lim_{k\to\infty} \sigma_k = 0$, meaning that only a finite number of significant modes effectively contribute to field generation or reception.

If the total source energy is bounded by $\hat{E}$, the admissible current distributions lie inside a hypersphere of radius $\sqrt{\hat{E}}$. The operator $\mathcal{A}$ maps this hypersphere to an ellipsoid in the field space Y, whose kth semi-axis length is $\sigma_k\sqrt{\hat{E}}$. Each point on the hypersphere corresponds to a specific current distribution, while each point on the ellipsoid corresponds to a radiated field pattern generated by that distribution.

Geometrically, each ϵ-ball within this ellipsoid represents one distinguishable radiation pattern or waveform under a fixed resolution ϵ. Non-overlapping ϵ-balls correspond to error-free distinguishable patterns, whereas overlapping balls correspond to partially correlated or error-tolerant cases. When all balls are non-overlapping, the ϵ-covering becomes an ϵ-packing problem, indicating perfect distinguishability. The total number of non-overlapping ϵ-balls represents the effective Kolmogorov ϵ-capacity of the operator $\mathcal{A}$.

This geometric representation directly unifies SIT and KIT. In SIT, distinguishable codewords are separated by the noise-limited uncertainty region; in KIT, resolvable field functions are separated by the deterministic resolution ϵ. Both can be interpreted as packing problems in the same function space. The number of non-overlapping ϵ-balls (or, equivalently, the number of dominant singular values above the noise or resolution threshold) defines the effective DoF of the channel. These DoFs characterize how many independent field modes can be excited or observed, providing a geometry- and physics-aware measure of the communication resources available in HMIMO systems.

B. Reinterpreting DoF in SIT/KIT

HMIMO systems, characterized by large and continuous apertures, naturally lend themselves to a functional-analytic treatment under the EIT framework. From the perspective of compact Hilbert–Schmidt operators, the spatial DoF correspond to the number of significant singular values (or eigenmodes) whose energy exceeds a prescribed threshold. This formulation directly connects (i) Shannon's probabilistic notion of noise-limited resolvability, (ii) Kolmogorov's deterministic ε-resolution, and (iii) the spectral concentration principles such as those of Landau–Pollak and Slepian for space–bandlimited functions. The result is a physically meaningful and geometry-dependent characterization of DoF that applies across both near- and far-field regimes.

Following the framework in [24], the spatial DoF depends jointly on the array domain $\mathcal{S}$ (the physical region supporting the excitation) and the solid angle $|\Omega|$ (the angular region over which radiated fields are observable). For electrically large systems where $\mathcal{S}|\Omega| \to \infty$, the asymptotic DoF scales as

$$\mathcal{N}^{\text{space}} \approx \mathcal{S}|\Omega|. \tag{38}$$

Typical geometries include $\mathcal{S} = 2L$ for a linear array of length $2L$, $\mathcal{S} = 2R$ for a circular array of radius R, and $\mathcal{S} = \pi R^2$ for a spherical aperture of radius R. For a transceiver pair with apertures $(\mathcal{S}_t, \mathcal{S}_r)$ and observable solid angles $(|\Omega_t|, |\Omega_r|)$, the overall DoF is limited by the weaker of the two links:

$$\mathcal{N}^{\text{space}} = \min\left\{\mathcal{S}_t|\Omega_t|,\, \mathcal{S}_r|\Omega_r|\right\}. \tag{39}$$

Additional DoF can arise from polarization diversity—e.g., dual- or tri-polarized arrays effectively multiply the spatial DoF by the number of independent polarization channels.

Considering two linear receivers with apertures $L_{r,1} > L_{r,2}$ and identical solid angles $|\Omega_1| = |\Omega_2|$ communicating with the same planar HMIMO transmitter of aperture $\mathcal{A}_t$ and solid angle $|\Omega_t|$. The resulting DoFs are

$$\begin{aligned}\mathcal{N}^{\text{space}}_{(1)} &= \min\left\{\mathcal{S}_t|\Omega_1|,\, L_{r,1}|\Omega_t|\right\},\\ \mathcal{N}^{\text{space}}_{(2)} &= \min\left\{\mathcal{S}_t|\Omega_2|,\, L_{r,2}|\Omega_t|\right\}.\end{aligned} \tag{40}$$

If the transmit DoF is the bottleneck ($\mathcal{S}_t|\Omega_1| < L_{r,2}|\Omega_t|$), enlarging the receiver aperture does not increase DoF; otherwise, the larger receiver supports more resolvable spatial modes. This mirrors the dual limitation between time duration and bandwidth in classical SIT [110].

Furthermore, as established in Sec. IV, the DoF can be reformulated as an ϵ-packing problem in the joint space–wavenumber domain $\mathcal{A}\times\Omega$. Let $\beta_d = \pi^{d/2}/\Gamma\left(\frac{d}{2}+1\right)$ be the volume of a d-dimensional unit ball. For characteristic spatial extents $(\delta_x, \delta_y, \delta_z)$ along three axes, the DoF is

$$\mathcal{N}^{\text{space}} = \frac{\mathrm{m}(\mathcal{S}\times\Omega)}{\beta_d\left(\frac{\delta_x}{2}\right)\left(\frac{\delta_y}{2}\right)\left(\frac{\delta_z}{2}\right)}, \tag{41}$$

where $\mathrm{m}(\cdot)$ denotes the joint measure of the aperture–spectral region. This expression reinforces that DoF increases with both physical aperture $\mathcal{S}$ and solid angle $|\Omega|$. However, practical constraints often limit aperture expansion; thus, enlarging the effective solid angle—via relays, distributed arrays, or cooperative reflection surfaces—offers a more feasible means of boosting DoF. In rich scattering environments, additional multipath components further enlarge $|\Omega|$ by providing distinct angular clusters, each contributing new resolvable spatial modes.

Physically, in multipath or distributed environments, each distinguishable propagation path can be interpreted as a separable mode in the operator domain. Paths are distinct if they occupy non-overlapping angular subspaces, jointly defining the channel rank [111]. Increasing antenna spacing enlarges the set of resolvable virtual angles and hence spatial diversity, but overly wide spacing may introduce inter-cluster interference from angular overlap. In far-field LoS channels, the critical sampling interval is approximately $\lambda/2$ for infinite apertures, while finite apertures may tolerate slightly larger spacings [78]. This tolerance is not a design recommendation: to avoid spatial aliasing and to suppress grating lobes, HMIMO systems therefore operate in an intentionally oversampled regime to preserve high spatial resolution and mitigate aliasing. In near-field or rich NLoS cases, the spatial DoF increases with both the array size and the angular richness of the environment.

The DoF concept provides a unifying performance metric for different functional objectives and transceiver implementations. This is because DoF characterizes the maximum number

Authorized licensed use limited to: Zhejiang University. Downloaded on May 24,2026 at 03:23:22 UTC from IEEE Xplore. Restrictions apply.

of independent resolvable signal dimensions (communication modes) that a system can reliably support, and these dimensions can be explicitly structured and flexibly allocated depending on system goals.

For example, in joint communication–imaging systems, the total DoF N_0 can be decomposed into communication and imaging sub-resources, i.e., $N_0 = N_0^{\text{comm}} + N_0^{\text{imag}}$, offering direct intuition for balancing data throughput and imaging resolution. Building on this resource-allocation perspective, in multi-user HMIMO, DoF further admits a physical interpretation as the number of resolvable spatial eigenmodes (eigen-channels). This structural interpretation determines the largest subspace dimension over which independent spatial communication modes can be multiplexed with asymptotically vanishing inter-mode interference at high SNR, clarifying its role as a system-level interference-management bound.

In wideband HMIMO implementations, the effective DoF dimension also offers practical intuition for the minimum number of controllable spatial signal paths needed for beam-squint-robust precoding design in high-SNR regimes. While this is related to the number of active RF chains, it should be interpreted as a reference lower bound rather than a strict equality, since RF chains represent hardware realizability, whereas DoF describes resolvable signal dimensions in the EM channel. Guided by the principle that subspace dimension is preserved under unitary basis transforms, precoders can be designed to operate on a dominant DoF-spanning mode set (or a DoF-preserving bandwidth partition), enabling approximately inter-mode-interference-free and beam-squint-mitigated signaling, while significantly reducing the complexity of mode optimization.

Finally, since DoF fundamentally measures resolvable signal dimensions rather than fixed hardware, these dimensions can be expanded through physical channel engineering. Specifically, programmable scatterers or active illumination can synthesize or unlock additional resolvable spatial modes, increasing the effective DoF in both near- and far-field propagation. DoF is simultaneously a theoretical dimensionality limit, a precoding/interference management principle, and a scalable architectural guideline that informs both the minimum hardware needed to preserve resolvable dimensions and the physical means to enlarge them.

Therefore, the spatial DoF thus serves as a unifying bridge between SIT/KIT-based information measures and physically realizable channel behavior. It encapsulates how geometry, aperture, and angular richness jointly determine the information-carrying capacity of HMIMO systems, providing a rigorous and physically grounded foundation for subsequent system optimization.

C. Wideband and Dual-Wideband Effects

Having established the spatial DoF interpretation under quasi-monochromatic excitation in the previous subsection, we now extend the analysis to broadband HMIMO systems, where temporal–spectral dimensions interact with spatial modes. Such systems naturally exhibit *wideband* and *dual-wideband* effects that reshape both the physical propagation behavior and the information-theoretic DoF budget.

Wideband transmission enables higher data rates and stronger robustness to multipath fading by exploiting additional spectral DoFs in the frequency domain. Multiple data streams can thus be multiplexed over independent subcarriers, making wideband and ultra-wideband HMIMO architectures particularly attractive for 6G communications.

However, the classical narrowband assumption—that the time delay τ_m across array elements satisfies $s(t-\tau_m) \approx s(t)$ for $T_s \gg \tau_m$—no longer holds when both bandwidth and aperture size become large. As the array aperture increases, the propagation delay difference between the reference and edge elements becomes comparable to the signal duration or the inverse bandwidth. In this case, different antenna elements receive time-shifted versions of the waveform rather than instantaneous samples of the same signal. The resulting non-negligible delay difference across the array induces an intrinsic *spatial-wideband effect* (or spatial selectivity), which is distinct from the conventional *frequency-wideband effect* (frequency selectivity) caused by multipath delay spread. When both phenomena coexist, the system experiences *dual-wideband effects* that jointly couple spatial and temporal domains.

As summarized in [112], dual-wideband effects introduce several challenges. The frequency-wideband effect reduces coherence bandwidth, leading to inter-symbol interference, while the spatial-wideband effect causes beam squint, beam split, and defocus [113]. These effects complicate beam alignment and decoding processes, and hence require either (i) *algorithm-based* mitigation (e.g., precoding or phase-compensation schemes) or (ii) *architecture-based* mitigation (e.g., true-time-delay hardware).

Representative modeling efforts [114] describe the dual-wideband channel using three coupled factors: a spatial steering vector (array response over angles), a frequency steering vector (subcarrier response to delay), and a phase-shift matrix (path diffusion effects). Applying a 2D inverse Fourier transform to the spatial–frequency domain yields the angular–delay domain representation. Under the planar-wave assumption, the angular–delay map exhibits a rectangular shape in the far field [112]; under the spherical-wave assumption, it becomes diamond-shaped in the near field [115], reflecting stronger angular–frequency coupling.

To date, dual-wideband phenomena have rarely been studied within EM-compliant channel models (see Sec. V). Traditional formulations remain based on discrete planar or spherical assumptions. In contrast, Green's function–based models inherently account for propagation delay through their exponential phase kernel, thereby offering a more faithful description of beam squint, delay squint, and diffusion phenomena. The resulting frequency-dependent angular spread can be directly computed and observed, enabling a physically consistent quantification of wideband effects within the EIT framework.

In summary, dual-wideband effects do not merely impair system performance; they fundamentally reshape the coupled spatio–spectral DoF landscape. From an EIT perspective, they highlight the necessity of jointly modeling time, frequency, and spatial variables as a unified information space, motivating

Authorized licensed use limited to: Zhejiang University. Downloaded on May 24,2026 at 03:23:22 UTC from IEEE Xplore. Restrictions apply.

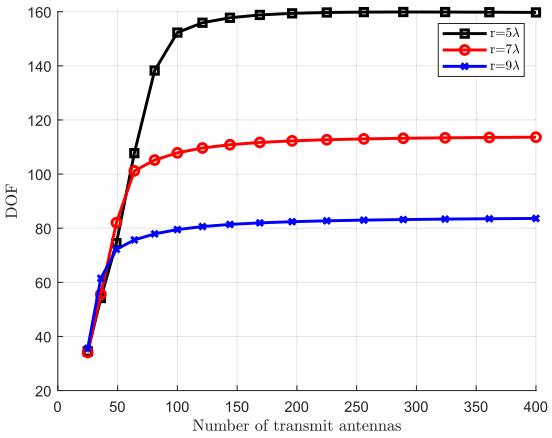

Fig. 13. DoF v.s. number of antennas within the fixed transmit surface at different distances r.

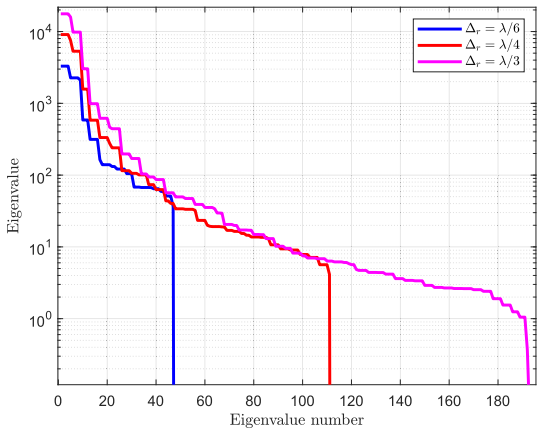

Fig. 14. Eigenvalues of far-field NLoS HMIMO systems for different spacing at the receiver.

co-design across algorithmic (precoding/compensation) and architectural (true-time-delay) dimensions in future HMIMO systems.

VII. Numerical Evaluation

In this section, the performance of the EM-compliant HMIMO models is analyzed using MATLAB simulations. Specifically, two performance metrics, namely DoF and capacity, are employed to assess HMIMO systems across different scenarios.

A. DoF and Eigenvalues Evaluation

Considering a fixed surface area, continuously increasing the number of antennas does not always yield a proportional improvement in DoF. The DoF eventually saturates due to the deformation of antenna patterns caused by strong mutual coupling, as shown in Fig. 13. The figure illustrates the DoF of the generated LoS channel, computed as $(\mathrm{tr}(\mathbf{R})/\|\mathbf{R}\|_F)^2$, where $\mathbf{R}$ denotes the channel correlation matrix obtained for varying numbers of transmit antennas. This computation provides a physically consistent interpretation with [116], where DoF is defined as the number of eigenvalues exceeding half of the largest one. The HMIMO surface area is $64\lambda^2$ (square shape), and we consider transmitter-receiver distance at $r = 5\lambda, 7\lambda$ and 9λ, respectively. From the figure, it is evident that HMIMO in the near field exhibits the highest DoF, primarily because the third polarization component possesses the strongest power. However, as the distance increases, the near-field region moves to the far-field region, resulting in a considerable decrease in DoF. Additionally, the DoF does not continuously improve with an increasing number of transmit antennas. This behavior can be attributed to the distorted antenna pattern and the strong coupling effects.

An intriguing finding from [52] suggests that moderate mutual coupling may slightly alter the effective DoF by perturbing the radiation pattern and exciting additional weak modes. However, excessive coupling (i.e., very small inter-element spacing) increases spatial correlation and leads to DoF degradation. Furthermore, the spatial DoF of aperture-constrained HMIMO systems is approximately proportional to the physical surface area for both far-field and near-field regimes [117], [118]. This relationship originates from the aperture's space–bandwidth product: a larger physical surface supports a wider range of tangential wavenumbers, thereby enabling more resolvable field modes. It should be noted that this DoF scaling is geometric and spectral in nature rather than power-driven—changes in transmit/receive power affect mode detectability but not the intrinsic DoF itself.

Recent studies have further extended DoF characterization toward more practical formulations. For instance, [119] introduces a directivity-aware model where antenna radiation patterns and element spacing jointly determine the uneven distribution of coupling coefficients in the wavenumber domain, from which the effective DoF is evaluated via cumulative energy thresholds. Meanwhile, [120] develops an analytical framework for near-field XL-MIMO based on the Green's function representation, expressing the effective DoF in closed form through the ratio of the operator trace and Frobenius norm. These works complement the geometric and spectral interpretations discussed above by offering direct analytical or statistical quantification of effective DoF in realistic array configurations.

The eigenvalue of far-field NLoS HMIMO channels for different spacing at the receiver is depicted in Fig. 14. The figure shows an uneven distribution of coupling coefficient intensities. The initial eigenvalues are substantial but rapidly converge towards zero, indicating the emergence of spatial correlation within the far-field HMIMO channel. The more uneven the coupling coefficients and the steeper the eigenvalues decay, which implies a stronger correlation and less DoF. In addition, smaller antenna spacing leads to stronger coupling effects, resulting in fewer dominant eigenvalues and diminished corresponding strengths. To provide an example, the HMIMO configuration with a spacing of $\lambda/6$ exhibits a smaller number of nonzero eigenvalues and weaker strengths when compared to the $\lambda/4$ and $\lambda/3$ cases.

The eigenvalue characteristics of near-field LoS HMIMO channels, as depicted in Fig. 15, are notably more intricate compared to those of far-field NLoS HMIMO channels illustrated in Fig. 14 due to the involvement of polarized

Authorized licensed use limited to: Zhejiang University. Downloaded on May 24,2026 at 03:23:22 UTC from IEEE Xplore. Restrictions apply.

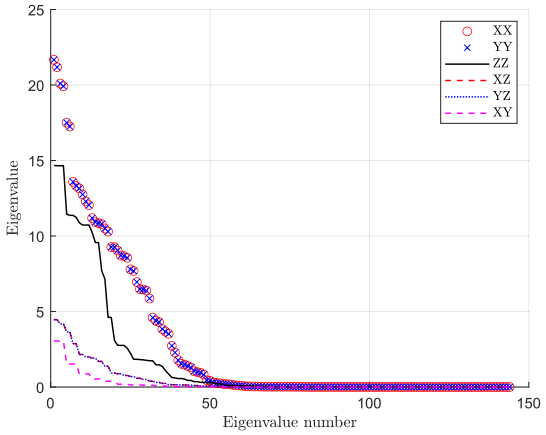

Fig. 15. Eigenvalues of near-field LoS HMIMO systems for co-polarized and cross-polarized channel components at distance $r = \lambda$.

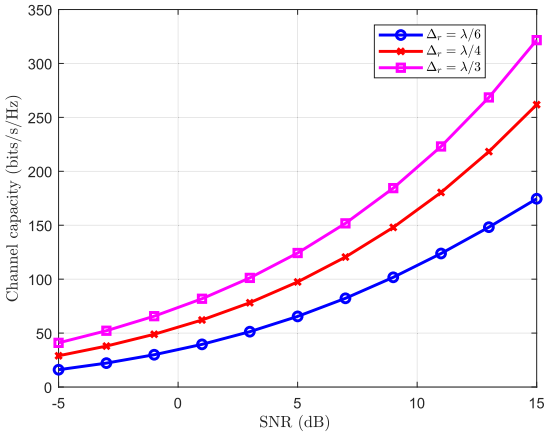

Fig. 16. Capacity of far-field NLoS HMIMO scheme for different spacing at the receiver.

components, which involves co-polarized channels (XX, YY, and ZZ polarized components) and cross-polarized channels (XY, YZ, and XZ polarized components). It can be observed from the figure that the third co-polarized component (ZZ) in the near field displays dominant values similar to the other two co-polarized components (XX and YY). In addition, the eigenvalues of cross-polarized components retain non-zero values, which degrades the performance (e.g., DoF and capacity).

B. Capacity Evaluation

The capacity is defined as the maximum mutual information, and the mutual information is the uncertainty reduced by observations [15]. In order to measure the capacity of continuous-space communication channels, the basis functions can be employed to approximate continuous space in transmitter and receiver [82], then the input-output relationship is represented in discrete forms with mappings between transmit and receive eigenfunctions, thus facilitating the capacity with finite eigenfunctions. A similar method is adopted in [33], where the current density and generated field are decomposed in orthogonal basis functions. It analyzed the mutual information and the capacity through spatial spectral density for random EM fields between two continuous regions, and simulation results proved the suboptimality of the half-wavelength sampling.

To improve the tractability and physical relevance of capacity analysis, multiple physical constraints are incorporated. For instance, the radiated-power constraint alone is insufficient, and an additional source-current constraint is imperative for deriving physically realizable capacity limits [28]. In practice, this constraint bounds the total surface current energy, e.g., $\int_S \|\mathbf{J}(\mathbf{r})\|^2 dS \leq J_{\max}^2 S$, ensuring that the current distribution $\mathbf{J}(\mathbf{r})$—which generates the field through the dyadic Green's operator—remains physically feasible under material and amplifier limitations. This necessity arises from the non-unique mapping between radiated power and source excitation; that is, a bounded radiated power does not necessarily correspond to a bounded source L^2 norm. By jointly incorporating both the source L^2-norm and radiated-power constraints, the work

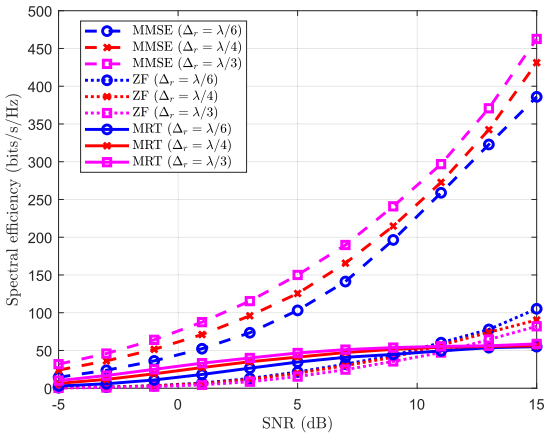

Fig. 17. Spectral efficiency of far-field NLoS HMIMO scheme with MMSE, ZF, and MRT precoding schemes for different spacing at the receiver.

in [28] maximizes the mutual information between source distributions and the observed field, leading to a more practical estimate of capacity. Building upon this foundation, [121] further investigates physical capacity bounds for canonical shapes such as plates, disks, cylinders, and spheres, while [63] introduces the Q-factor constraint to account for the bandwidth limitation of antenna arrays. Nevertheless, current capacity analyses in wireless communications remain predominantly environment-centric, often overlooking the influence of antenna design; hence, integrating such physical constraints into wireless capacity theory is still an open and evolving research direction.

In the following, we will provide numerical capacity analysis for far-field and near-field HMIMO systems.

1) Capacity of Far-Field NLoS HMIMO: The channel capacity for far-field HMIMO systems with varying spacing at the receiver is depicted in Fig. 16. The less spacing has a lower capacity due to the stronger coupling effects. For example, the curve with spacing $\lambda/6$ achieves 180 bits/s/Hz at a SNR 15dB. To mitigate the impact of spatial correlation, effective precoding techniques become imperative. Three predominant conventional methods are commonly employed: minimum mean square error (MMSE), zero-forcing (ZF), and

Authorized licensed use limited to: Zhejiang University. Downloaded on May 24,2026 at 03:23:22 UTC from IEEE Xplore. Restrictions apply.

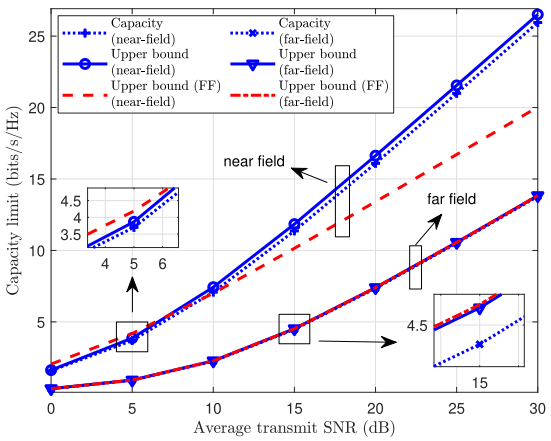

Fig. 18. Capacity limit versus the transmit average SNR in LoS scenarios.

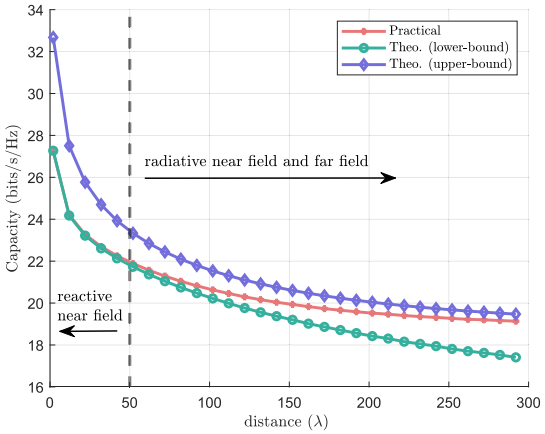

Fig. 19. The comparison of the practical channel capacity and theoretical capacity at varying transceiver distances from 2λ to 300λ.

maximum ratio transmission (MRT) schemes. The spectral efficiency of HMIMO systems equipped with these three linear techniques are shown in Fig. 17. The MMSE scheme outperforms ZF and MRT because it provides a balanced trade-off between interference suppression and noise amplification. In correlated HMIMO channels with limited receiver spacing, MMSE remains robust against channel ill-conditioning, whereas ZF suffers from noise enhancement and MRT fails to mitigate multi-stream interference. Clearly, incorporating such schemes could greatly enhance spectral efficiency. However, it's important to note that due to the compact antennas utilized in HMIMO systems, the implementation of precoding schemes entails resource-intensive operations, particularly in cases involving matrix inversions, such as MMSE and ZF precoding methods, and the exploration of efficient precoding designs remains an ongoing area of investigation.

2) Capacity of Near-Field LoS HMIMO: Based upon the relation between the electric field and current distribution in (9), the communication model can be reformulated based on the DGF, and then we can derive the upper bound of capacity by considering a uniform power allocation scheme for all independently parallel transmission channels. More details can be found in [35]. The demonstration of channel capacity and its upper bound in both near field and far field cases are given in Fig. 18. As seen from the figure the capacity in the near-field region is higher than that in the far-field region, and it is proportional to the SNR. We then observe that the derived upper bound provides an effective and tightness bound for the exact capacity in both near-field and far-field scenarios. Besides, the traditional far-field upper bound is incapable of providing an effective bound on the exact capacity, especially for the near-field region.

The theoretical bound in continuous transceiver distances is given in Fig. 19, where the channel is modeled through SDG functions. It can be observed that the theoretical lower bound perfectly matches the practical channel model in the reactive near-field region and the theoretical upper bound predicts the channel capacity in the radiative near-field and far-field zones, thus validating the effectiveness of the theoretical analysis.

In addition, the complex spatial and polarization correlation in near-field communications requires effective beamforming design [122], [123], [124]. It is proved that the power gain using conventional beamforming is suboptimal to that in near-field beamfocusing using the spherical wave channel model [94]. When considering to exploit the polarization diversity in near field, the work [96] proposed a two-layer precoding scheme. Specifically, a Gaussian elimination method was adopted to eliminate polarization interference and a block diagonalization method was employed to remove inter-user interference. However, such a method requires higher computational complexity, and an unequal efficient power allocation scheme is necessary due to the power imbalance in the three polarizations.

As demonstrated above, the DoF and capacity of both far-field and near-field HMIMO can be substantially enhanced through various approaches. These include expanding the surface area of transmitters/receivers, integrating near-field communication strategies, and leveraging advanced precoding/beamforming techniques. However, it is important to acknowledge certain limitations. For example, the compact antennas installed in HMIMO systems require sophisticated and costly precoding/beamforming strategies, which necessitate in-depth exploration.

C. Sphere-Packing Solution

As presented in the former section, both DoF and capacity measurement in SIT/KIT framework can be transformed into sphere-packing problems. Therefore, we will evaluate the performance with power constraints through the sphere-packing solution in this part.

Specifically, the emitted power within a specified area is constrained to remain below a certain threshold. Consequently, parts of DoF are allocated to limit the energy radiation range, i.e., pattern constraint, while the remaining DoF is utilized for information transmission. Notably, such power constraint decreases the overall capacity of the system. Thus, the balance between energy transmission and information transmission becomes critical in optimizing the system's performance.

Fig. 20 illustrates the transmission between a 10λ linear electric source and a 6λ observation line separated by a distance of 10λ (source codes from [125]). In Fig. 20 (a),

Authorized licensed use limited to: Zhejiang University. Downloaded on May 24,2026 at 03:23:22 UTC from IEEE Xplore. Restrictions apply.

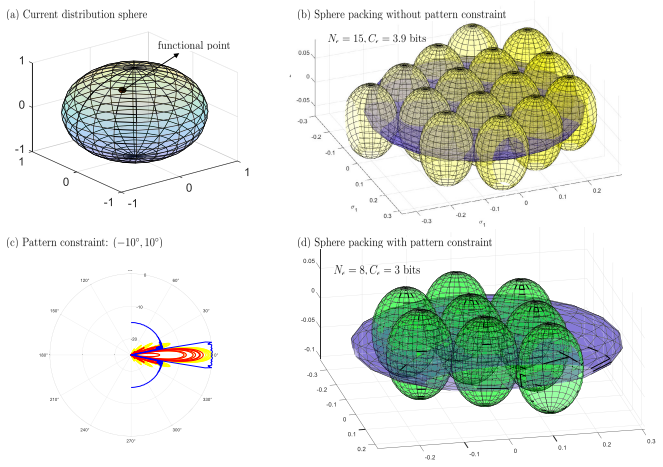

Fig. 20. The electric line with length 10λ and the linear observation line with length 6λ for distance 10λ. (a) current distribution sphere; (b) sphere packing without pattern constraint; (c) pattern constraint: $(-10°, 10°)$; and (d) sphere packing with pattern constraint (source codes from [125]).

each functional point in the sphere represents the specific current distribution. Through the compact operator $\mathcal{A}$, each functional is transformed into a sphere in the field ellipsoid, and there are 15 non-overlapping balls, thus the capacity is 3.9 bits [Fig. 20 (b)]. However, if imposing pattern constraints, e.g., the radiation pattern outside $(-10°, 10°)$ is set to below a certain value [Fig. 20 (c)], then the capacity would be reduced to 3 bits since there are 7 distinguishable waveforms do not meed pattern constraint [Fig. 20 (d)].

It is imperative to acknowledge that superdirective HMIMO systems are exceptions. Specifically, a superdirective source permits the presence of arbitrarily high reactive energy. Consequently, the resulting radius of the source hyper-ball $\hat{E}$ could become substantially large. In such a configuration, even the small singular values of the integral operator $\mathcal{A}$ may make significant contributions to communications, especially for large semi-axis $\sigma_k \hat{E}$ within the ellipsoid Y [26]. As a result, the superdirective source has the potential to achieve theoretically high ϵ-entropy.

VIII. Future Research Directions

The HMIMO-oriented EIT introduces novel opportunities for exploring performance within the framework of practical physical constraints. In this context, we offer insights for prospective research directions in EIT for HMIMO systems.

A. Mechanism of EM Environment Control and Interactions

Utilizing HMIMO systems to offer significant flexibility and adaptability for achieving multiple communication goals across various scenarios is a complex task, necessitating a thorough examination of the mechanisms that govern favorable environment regulation and interactions.

To begin, it is important to note that HMIMO systems are expected to improve performance (e.g., DoF, capacity, and channel rank) substantially while bringing difficulty in environment control. However, such improvement introduces complexities in environmental control. For example, rotating the HMIMO plane may bring more benefits in terms of capacity compared to spreading it over a wide area, as shown in [126]. In addition, harnessing the unevenly spaced patch antennas over HMIMO to control complicated EM environments is also anticipated while remaining untapped.

Moreover, investigating the optimal number of patch antennas for environment regulation over HMIMO systems appeals to research interests, since constructing a continuous structure is impractical. Specifically, the performance gain (e.g., DoF, capacity) ceases to increase constantly with the increase of the number of patch antennas [52], [96], [127]. However, theoretically analyzing the optimal number of antennas given a fixed area is not fully investigated yet.

In essence, the intricacies of managing the EM environment, along with its associated wave interactions, remain unresolved, not to mention the related real-time control and security issues.

B. Design and Implementation of 3D HMIMO-Based Superdirective Antennas

Newly envisioned architectures, i.e., 3D HMIMO-based superdirective antennas, are expected to break EM limits such as the Hannan limit, and demonstrate remarkable potential in capacity enhancement. Nevertheless, the pursuit of such designs encounters several formidable challenges. Primarily, combating the serious energy efficiency loss inherent in such a structure is imperative. Different from traditional 1D (linear) and 2D (planar) antenna arrays, the individual patch antenna in 3D HMIMO systems suffers from much more severe coupling effects stemming from surrounding patch antennas in 3D space, resulting in excessively low energy efficiency and array gain. Consequently, devising 3D HMIMO-based superdirective antennas remains an unresolved quandary. Moreover, while the promising superdirectivity is anticipated to cater to practical scenarios in the context of 3D HMIMO-based antennas, a suitable matching network is difficult to implement. More precisely, within such a 3D framework, perfectly matching the input impedance and output impedance is problematic in transferring almost all power to the load. Therefore, from the perspective of hardware realization, designing an effective feed circuit and matching network are challenging in achieving 3D superdirective HMIMO.

C. Efficient Field Sampling Schemes

Despite the existence of various field sampling methods, such as uniform and nonuniform, planar and spherical sampling, an optimal sampling method that can accurately approximate the field with the minimum number of sampling points has not been determined yet.

First, it should be noted that the optimal sampling method in the far-field zone may differ from that in the near-field region. While the conventional half-wavelength rectangular sampling method is less effective than (elongated) hexagonal sampling methods in the far-field zone due to the inclusion of extra information (reactive energy) [80], this does not necessarily imply that the conventional rectangular sampling method is also ineffective in the near-field zone. Furthermore, it is important

Authorized licensed use limited to: Zhejiang University. Downloaded on May 24,2026 at 03:23:22 UTC from IEEE Xplore. Restrictions apply.

to explore other sampling values in the rectangular sampling method. For instance, considering a sampling interval less than $\lambda/2$ outside a specified region may prove to be more effective in capturing critical information in certain scenarios.

Next, the utilization of a nonuniform sampling method holds promise for reducing the number of samples required. The author in [128] proposed a nonuniform random sampling method for sparse EM sources to reduce the number of measure data with the aid of a priori information. The space dimension is initially reduced, and the amount of information is then evaluated using Kolmogorov ϵ-entropy. The findings substantiate that nonuniform sampling proves more effective than the conventional $\lambda/2$ equispaced sampling strategy when employing geometrical data. Although nonuniform sampling has demonstrated its effectiveness, the problem of designing sampling patterns in the near-field and far-field zones is still in the early stages of research. It is suggested that incorporating geometrical information of the source and surrounding environment may prove beneficial in designing a cost-efficient yet effective nonuniform sampling strategy.

D. Impacts of Scatterers and EM Noise

The current performance analysis for HMIMO systems is mainly categorized into two types: conventional MIMO analysis and antenna analysis. In traditional MIMO analysis, the mutual coupling and polarization effects are normally modeled as a random process, simplifying the analysis using probabilistic assumption while neglecting the physical influences, such as multi-path and scattering environments, resulting in the underestimation of HMIMO performance, such as capacity and power gain. On the other hand, antenna analysis takes radiation patterns and efficiencies into consideration. However, this approach falls short of offering a complete interpretation of communications in a more explicable manner. For example, although the Q factor and directivity gain describe the performance of antenna systems in practical deployment, the information content from the perspective of communications in such a setting is still unclear. Therefore, integrating the above concerns into EIT is still challenging, and the complex environment further increases the difficulty of related analysis.

Primarily, multiple scatterers can be present, resulting in the propagation of EM waves from the transmitter to the receiver through various paths. Each scatterer also acts as a secondary source, further contributing to the radiation of EM waves. However, many existing works in antenna analysis tend to focus solely on the direct link between the transmitter and receiver, disregarding the presence and impact of scatterers. In these analyses, dyadic or scalar Green's functions are often employed to model the transmission process. The involvement of secondary sources or higher-order sources is only discussed in very few works [129], [130], [131], despite their common occurrence in wireless communications.

Furthermore, noise modeling in traditional MIMO systems typically assumes Gaussian variables. However, in the context of EM noise, the scenario becomes more intricate, encompassing radiation interference from undesired sources and measurement noise stemming from physical antenna configurations. Given the complexity of EM noise, it is essential to properly address noise modeling in performance analysis and applications. Accurate noise modeling allows for a more realistic evaluation of system performance, leading to the development of effective encoding and modulation schemes that can mitigate the impact of noise in HMIMO systems.

E. Accurate Capacity Region Evaluation

The precise representation of the capacity region is significant in quantifying HMIMO systems, however, several unsolved problems persist in the evaluation process, especially for near-field HMIMO communications.

First of all, the EM waves interaction in the near-field region is complicated to be numerically described. As previously discussed, unlike the planar waves in the far-field zone, there are numerous spherical waves in the near-field region, incorporating rich information on phase and distance. Therefore, measuring such information accurately is laborious. Typically, the truncation methods are employed to represent the near-field region with a finite number of dominant waves, aiming at reducing the computational complexity. However, determining the number of dominant modes in near-field communications is normally infeasible, and improper truncation would introduce notable approximation errors. Under such a circumstance, the capacity region depiction of near-field HMIMO systems becomes a formidable task.

In addition, near-field HMIMO is anticipated to exhibit excellent superdirectivity, yielding excessively high radiation power, and enabling abundant encoding/decoding schemes. Nevertheless, the traditional capacity region technique is not applicable due to the consideration of inexhaustible scheduling policies in the derivation of optimal capacity region.

Lastly, the channel in traditional communications is modeled as a probabilistic process characterized by means and variances, resulting in direct computation of the channel's eigenvalues and facilitating capacity region evaluation. Nonetheless, this modeling approach may overlook the antenna configuration and fail to fully interpret the physical environment, leading to an erroneous estimation of capacity.

F. Excitation/Field Encoding and Modulation

To minimize temporal costs, it is essential to fully exploit the available spatial resources. The information content carried by the field can be measured by DoF, representing the number of distinguishable patterns. Each pattern corresponds to an independent information component that is generated through the manipulation of current density. Therefore, exploring the linear or nonlinear relationship between the excitation current and the resulting radiated field is of particular interest. However, there are three main issues that need to be addressed in this research.

First, it is essential to note that the optimal current distribution is generally not unique, i.e., each pattern can be excited by multiple possible excitations. As a result, the mapping from the current distribution to the specified antenna pattern is not definitively defined. To address this issue, the problem can be divided into two steps. In the first step, the goal is to find the available excitations based on the kernel functions and the

Authorized licensed use limited to: Zhejiang University. Downloaded on May 24,2026 at 03:23:22 UTC from IEEE Xplore. Restrictions apply.

desired pattern. Subsequently, in the second step, the objective current distribution is derived by employing mathematical methods and considering physical constraints.

Then, the distinguishable field also depends on the surrounding environment and physical configuration. The radiation pattern, for instance, can exhibit variations in the near-field zone compared to the far-field region, especially for evanescent waves. Additionally, closely spaced antennas may lead to radiation pattern deformations, causing certain patterns to become indistinguishable from others. As a result, it is crucial to take these physical constraints into account during antenna design. By incorporating these constraints, the effectiveness of the encoding and modulation process can be enhanced. Through proper encoding scheme, the received signal can be retrieved from the distinguishable field patterns.

Furthermore, distinguishable patterns can be leveraged in spatial modulation techniques. For example, similar to index modulation, the index of excited field patterns can carry additional information beyond what is embedded in the individual excited patterns. Additionally, the polarization domain can be exploited in spatial modulation by combining different polarization states to convey more information. The spatial information itself can also contribute to the modulation process. For example, users at different locations may observe distinct waveforms, allowing for location-based information transmission. By incorporating these spatial modulation strategies, HMIMO systems can achieve more efficient and versatile data transmission, making use of the diverse characteristics of the spatial domain to enhance communication performance.

It should be noted that the superdirectivity source with arbitrarily high reactive energy is a unique case. Geometrically, consider an antenna enclosed within a sphere with an arbitrarily large energy radius $\hat{E}$. In this context, the ellipsoid generated from the operator $\mathcal{A}$ would have arbitrary large semi-axes, admitting high ϵ-entropy, i.e., C_ϵ. Theoretically, such a source could achieve an arbitrarily long length 2^{C_ϵ}-codebook without delay [25].

In addition to the aforementioned directions, there are still several other unmentioned research avenues to be explored, such as low-cost beamforming designs and activity detection methods in exploiting EM wave propagation. These unexplored areas present exciting opportunities for further research and development in HMIMO systems, promising advancements in the design, performance, and practical applications of these advanced wireless communication systems.

IX. Conclusion

We have conducted a comprehensive review of the HMIMO-oriented EIT framework, which systematically integrates information-theoretic principles with EM physical constraints to establish a unified understanding of HMIMO systems.

From the physical perspective, inevitable mutual coupling among sub-wavelength elements leads to reduced directivity and an increased quality factor, thus constraining bandwidth and radiation efficiency. Nevertheless, such strong coupling can also be exploited to realize superdirectivity, provided that element spacing and excitation distributions are carefully optimized to balance gain and efficiency.

At the EM characterization level, field-based formulations such as Green's function representations and near-/far-field decompositions reveal how EM propagation mediates the transfer of information through physical space. These formulations bridge the EM description and system modeling, providing a foundation for channel synthesis and DoF analysis.

Moving to field sampling and spatial DoF, we have emphasized that the EM field constitutes a continuous information carrier. Hence, the spatial sampling process—determined by the array geometry, aperture size, and element spacing—directly governs the number of resolvable modes. HMIMO surfaces, by approaching continuous apertures, enable spatial oversampling that captures higher-order spherical modes, thereby unlocking additional DoF beyond those accessible in conventional discrete MIMO arrays.

To elucidate the input–output relationship, several EM-compliant channel models were examined, including the Fourier plane-wave expansion, dyadic Green's function, and stochastic Green's function models. Each targets a specific regime—rich scattering, LoS-dominant, and arbitrary environments—with different computational complexities. Simulation-based evaluations confirm that larger apertures, wider element spacing, and shorter propagation distances yield greater DoF and capacity gains.

From the information-theoretic viewpoint, both the probabilistic SIT and deterministic KIT frameworks are applicable to temporal and spatial domains due to their inherent space–time duality. Yet, subtle asymmetries between the two domains necessitate the KIT as a complementary analytic tool to SIT, particularly for near-field scenarios and spatially continuous apertures. This unified SIT–KIT perspective reinterprets DoF as a measurable quantity rooted in physical field modes and enables rigorous evaluation of wideband and dual-wideband HMIMO systems.

In summary, the EIT framework bridges the gap between theoretical EM foundations and practical HMIMO implementations. It provides a consistent physics-based foundation for performance characterization, information measurement, and aperture design optimization. Despite the remaining challenges in fully realizing HMIMO-oriented EIT, this survey establishes a comprehensive foundation and highlights promising directions for future exploration in field-based channel modeling, space–time DoF quantification, and physics-compliant information processing.

Acknowledgment

Any opinions, findings and conclusions or recommendations expressed in this material are those of the author(s) and do not reflect the views of the Ministry of Education, Singapore.

References

[1] C. Volmer, J. Weber, R. Stephan, K. Blau, and M. A. Hein, "An eigen-analysis of compact antenna arrays and its application to port decoupling," *IEEE Trans. Antennas Propag.*, vol. 56, no. 2, pp. 360–370, Feb. 2008.

[2] D. W. Browne, M. Manteghi, M. P. Fitz, and Y. Rahmat-Samii, "Experiments with compact antenna arrays for MIMO radio communications," *IEEE Trans. Antennas Propag.*, vol. 54, no. 11, pp. 3239–3250, Nov. 2006.

Authorized licensed use limited to: Zhejiang University. Downloaded on May 24,2026 at 03:23:22 UTC from IEEE Xplore. Restrictions apply.

[3] D. Sipal, M. P. Abegaonkar, and S. K. Koul, "Easily extendable compact planar UWB MIMO antenna array," *IEEE Antennas Wireless Propag. Lett.*, vol. 16, pp. 2328–2331, 2017.

[4] D. K. Papantonis and J. L. Volakis, "Dual-polarized tightly coupled array with substrate loading," *IEEE Antennas Wireless Propag. Lett.*, vol. 15, pp. 325–328, 2016.

[5] A. O. Bah, P.-Y. Qin, R. W. Ziolkowski, Y. J. Guo, and T. S. Bird, "A wideband low-profile tightly coupled antenna array with a very high figure of merit," *IEEE Trans. Antennas Propag.*, vol. 67, no. 4, pp. 2332–2343, Apr. 2019.

[6] C. Huang et al., "Holographic MIMO surfaces for 6G wireless networks: Opportunities, challenges, and trends," *IEEE Wireless Commun.*, vol. 27, no. 5, pp. 118–125, Oct. 2020.

[7] H. Zhang, H. Zhang, B. Di, and L. Song, "Holographic integrated sensing and communications: Principles, technology, and implementation," *IEEE Commun. Mag.*, vol. 61, no. 5, pp. 83–89, May 2023.

[8] T. Gong et al., "Holographic MIMO communications: Theoretical foundations, enabling technologies, and future directions," *IEEE Commun. Surveys Tuts.*, vol. 26, no. 1, pp. 196–257, 1st Quart., 2024.

[9] J. An et al., "Stacked intelligent metasurface-aided MIMO transceiver design," *IEEE Wireless Commun.*, vol. 31, no. 4, pp. 123–131, Aug. 2024.

[10] J. An et al., "Stacked intelligent metasurfaces for efficient holographic MIMO communications in 6G," *IEEE J. Sel. Areas Commun.*, vol. 41, no. 8, pp. 2380–2396, Aug. 2023.

[11] J. An, C. Yuen, C. Huang, M. Debbah, H. V. Poor, and L. Hanzo, "A tutorial on holographic MIMO communications—Part III: Open opportunities and challenges," *IEEE Commun. Lett.*, vol. 27, no. 7, pp. 1674–1678, Jul. 2023.

[12] C. Huang, A. Zappone, G. C. Alexandropoulos, M. Debbah, and C. Yuen, "Reconfigurable intelligent surfaces for energy efficiency in wireless communication," *IEEE Trans. Wireless Commun.*, vol. 18, no. 8, pp. 4157–4170, Aug. 2019.

[13] Y. Liu et al., "Reconfigurable intelligent surfaces: Principles and opportunities," *IEEE Commun. Surveys Tuts.*, vol. 23, no. 3, pp. 1546–1577, 3rd Quart., 2021.

[14] L. Wei, C. Huang, G. C. Alexandropoulos, C. Yuen, Z. Zhang, and M. Debbah, "Channel estimation for RIS-empowered multi-user MISO wireless communications," *IEEE Trans. Commun.*, vol. 69, no. 6, pp. 4144–4157, Jun. 2021.

[15] C. E. Shannon, "A mathematical theory of communication," *Bell Syst. Tech. J.*, vol. 27, no. 3, pp. 379–423, Jul. 1948.

[16] D. Gabor, "Theory of communication. Part 1: The analysis of information," *J. Inst. Electr. Eng. III: Radio Commun. Eng.*, vol. 93, no. 26, pp. 429–441, Nov. 1946.

[17] D. Gabor, "Communication theory and physics," *Trans. IRE Prof. Group Inf. Theory*, vol. 1, no. 1, pp. 48–59, Feb. 1953.

[18] A. N. Kolmogorov and V. M. Tikhomirov, "ε-entropy and ε-capacity of sets in function spaces," *Uspekhi Matematicheskikh Nauk*, vol. 14, no. 2, pp. 3–86, 1959.

[19] O. Bucci and G. Franceschetti, "On the spatial bandwidth of scattered fields," *IEEE Trans. Antennas Propag.*, vol. AP-35, no. 12, pp. 1445–1455, Dec. 1987.

[20] O. M. Bucci and G. Franceschetti, "On the degrees of freedom of scattered fields," *IEEE Trans. Antennas Propag.*, vol. 37, no. 7, pp. 918–926, Jul. 1989.

[21] O. M. Bucci, C. Gennarelli, and C. Savarese, "Representation of electromagnetic fields over arbitrary surfaces by a finite and nonredundant number of samples," *IEEE Trans. Antennas Propag.*, vol. 46, no. 3, pp. 351–359, Mar. 1998.

[22] D. A. B. Miller, "Communicating with waves between volumes: Evaluating orthogonal spatial channels and limits on coupling strengths," *Appl. Opt.*, vol. 39, no. 11, pp. 1681–1699, 2000.

[23] R. Piestun and D. A. B. Miller, "Electromagnetic degrees of freedom of an optical system," *J. Opt. Soc. Amer. A, Opt. Image Sci.*, vol. 17, no. 5, pp. 892–902, 2000.

[24] A. S. Y. Poon, R. W. Brodersen, and D. N. C. Tse, "Degrees of freedom in multiple-antenna channels: A signal space approach," *IEEE Trans. Inf. Theory*, vol. 51, no. 2, pp. 523–536, Feb. 2005.

[25] M. D. Migliore, "On the role of the number of degrees of freedom of the field in MIMO channels," *IEEE Trans. Antennas Propag.*, vol. 54, no. 2, pp. 620–628, Feb. 2006.

[26] M. D. Migliore, "On electromagnetics and information theory," *IEEE Trans. Antennas Propag.*, vol. 56, no. 10, pp. 3188–3200, Oct. 2008.

[27] M. Franceschetti, M. D. Migliore, and P. Minero, "The capacity of wireless networks: Information-theoretic and physical limits," *IEEE Trans. Inf. Theory*, vol. 55, no. 8, pp. 3413–3424, Aug. 2009.

[28] F. K. Gruber and E. A. Marengo, "New aspects of electromagnetic information theory for wireless and antenna systems," *IEEE Trans. Antennas Propag.*, vol. 56, no. 11, pp. 3470–3484, Nov. 2008.

[29] M. Franceschetti, *Wave Theory of Information*, 1st ed., Cambridge, U.K.: Cambridge Univ. Press, Nov. 2017.

[30] M. D. Migliore, "Shannon and Kolmogorov in space communication channels," in *Proc. 14th Eur. Conf. Antennas Propag. (EuCAP)*, Mar. 2020, pp. 1–4.

[31] M. D. Migliore, "The world beneath the physical layer: An introduction to the deep physical layer," *IEEE Access*, vol. 9, pp. 77106–77126, 2021.

[32] S. S. A. Yuan, Z. He, X. Chen, C. Huang, and W. E. I. Sha, "Electromagnetic effective degree of freedom of an MIMO system in free space," *IEEE Antennas Wireless Propag. Lett.*, vol. 21, pp. 446–450, 2022.

[33] Z. Wan, J. Zhu, Z. Zhang, L. Dai, and C.-B. Chae, "Mutual information for electromagnetic information theory based on random fields," *IEEE Trans. Commun.*, vol. 71, no. 4, pp. 1982–1996, Apr. 2023.

[34] R. Ji et al., "Extra DoF of near-field holographic MIMO communications leveraging evanescent waves," *IEEE Wireless Commun. Lett.*, vol. 12, no. 4, pp. 580–584, Apr. 2023.

[35] T. Gong et al., "Holographic MIMO communications with arbitrary surface placements: Near-field LoS channel model and capacity limit," *IEEE J. Sel. Areas Commun.*, vol. 42, no. 6, pp. 1549–1566, Jun. 2024.

[36] C. Vanwynsberghe, J. He, and M. Debbah, "A universal framework for holographic MIMO sensing," 2023, *arXiv:2309.16389*.

[37] S. Mikki, "The Shannon information capacity of an arbitrary radiating surface: An electromagnetic approach," *IEEE Trans. Antennas Propag.*, vol. 71, no. 3, pp. 2556–2570, Mar. 2023.

[38] E. Björnson et al., "Towards 6G MIMO: Massive spatial multiplexing, dense arrays, and interplay between electromagnetics and processing," 2024, *arXiv:2401.02844*.

[39] J. Zhu, Z. Wan, L. Dai, M. Debbah, and H. V. Poor, "Electromagnetic information theory: Fundamentals, modeling, applications, and open problems," *IEEE Wireless Commun.*, vol. 31, no. 3, pp. 156–162, Jun. 2024.

[40] C.-X. Wang, Y. Yang, J. Huang, X. Gao, T. J. Cui, and L. Hanzo, "Electromagnetic information theory: Fundamentals and applications for 6G wireless communication systems," *IEEE Wireless Commun.*, vol. 31, no. 5, pp. 279–286, May 2024.

[41] J. Zhu, Z. Wan, L. Dai, and T. J. Cui, "Electromagnetic information theory-based statistical channel model for improved channel estimation," *IEEE Trans. Inf. Theory*, vol. 71, no. 3, pp. 1777–1793, Mar. 2025.

[42] C. E. Shannon, "Communication in the presence of noise," *Proc. IRE*, vol. 37, no. 1, pp. 10–21, Jan. 1949.

[43] D. Dardari and N. Decarli, "Holographic communication using intelligent surfaces," *IEEE Commun. Mag.*, vol. 59, no. 6, pp. 35–41, Jun. 2021.

[44] C.-X. Wang et al., "Modeling, capacity studies, antenna and system designs for 6G/B6G 3-D continuous-space radio channels enabled by electromagnetic information theory," *IEEE Commun. Surv. Tutor.*, vol. 28, pp. 1–63, 2026.

[45] M. D. Renzo and M. D. Migliore, "Electromagnetic signal and information theory," *IEEE BITS Inform. Theory Mag.*, vol. 4, no. 1, pp. 25–39, Jan. 2024.

[46] Y. Liu, C. Ouyang, Z. Wang, J. Xu, X. Mu, and Z. Ding, "CAPA: Continuous-aperture arrays for revolutionizing 6G wireless communications," *IEEE Wireless Commun.*, vol. 32, no. 4, pp. 38–45, Aug. 2025.

[47] Z. Wang et al., "A tutorial on extremely large-scale MIMO for 6G: Fundamentals, signal processing, and applications," *IEEE Commun. Surveys Tuts.*, vol. 26, no. 3, pp. 1560–1605, 3rd Quart., 2024.

[48] Z. Wang et al., "Extremely large-scale MIMO: Fundamentals, challenges, solutions, and future directions," *IEEE Wireless Commun.*, vol. 31, no. 3, pp. 117–124, Jun. 2024.

[49] H. Lu et al., "A tutorial on near-field XL-MIMO communications toward 6G," *IEEE Commun. Surveys Tuts.*, vol. 26, no. 4, pp. 2213–2257, 2024.

[50] M. Gustafsson and S. Nordebo, "Optimal antenna currents for Q, superdirectivity, and radiation patterns using convex optimization," *IEEE Trans. Antennas Propag.*, vol. 61, no. 3, pp. 1109–1118, Mar. 2013.

[51] Y. Zhao, Y. Hao, and C. Parini, "FDTD characterization of UWB indoor radio channel including frequency dependent antenna directivities," *IEEE Antennas Wireless Propag. Lett.*, vol. 6, pp. 191–194, 2007.

Authorized licensed use limited to: Zhejiang University. Downloaded on May 24,2026 at 03:23:22 UTC from IEEE Xplore. Restrictions apply.

[52] S. S. A. Yuan, X. Chen, C. Huang, and W. E. I. Sha, "Effects of mutual coupling on degree of freedom and antenna efficiency in holographic MIMO communications," *IEEE Open J. Antennas Propag.*, vol. 4, pp. 237–244, 2023.

[53] L. J. Chu, "Physical limitations of omni-directional antennas," *J. Appl. Phys.*, vol. 19, no. 12, pp. 1163–1175, Dec. 1948.

[54] R. Harrington, "On the gain and beamwidth of directional antennas," *IRE Trans. Antennas Propag.*, vol. 6, no. 3, pp. 219–225, Jul. 1958.

[55] R. F. Harrington, "Effect of antenna size on gain, bandwidth, and efficiency," *J. Res. Nat. Bur. Standards, Sect. D, Radio Propag.*, vol. 64D, no. 1, p. 1, Jan. 1960.

[56] M. Pigeon, C. Delaveaud, L. Rudant, and K. Belmkaddem, "Miniature directive antennas," *Int. J. Microw. Wireless Technol.*, vol. 6, no. 1, pp. 45–50, Feb. 2014.

[57] R. C. Hansen, "Fundamental limitations in antennas," *Proc. IEEE*, vol. 69, no. 2, pp. 170–182, Feb. 1981.

[58] P. Hannan, "The element-gain paradox for a phased-array antenna," *IEEE Trans. Antennas Propag.*, vol. AP-12, no. 4, pp. 423–433, Jul. 1964.

[59] P.-S. Kildal, A. Vosoogh, and S. Maci, "Fundamental directivity limitations of dense array antennas: A numerical study using Hannan's embedded element efficiency," *IEEE Antennas Wireless Propag. Lett.*, vol. 15, pp. 766–769, 2016.

[60] D. M. Pozar, "A relation between the active input impedance and the active element pattern of a phased array," *IEEE Trans. Antennas Propag.*, vol. 51, no. 9, pp. 2486–2489, Sep. 2003.

[61] S. S. A. Yuan et al., "Breaking the degrees-of-freedom limit of holographic MIMO communications: A 3-D antenna array topology," *IEEE Trans. Veh. Technol.*, vol. 73, no. 8, pp. 11276–11288, Aug. 2024.

[62] O. Onireti, A. Imran, and M. A. Imran, "Coverage, capacity, and energy efficiency analysis in the uplink of mmWave cellular networks," *IEEE Trans. Veh. Technol.*, vol. 67, no. 5, pp. 3982–3997, May 2018.

[63] C. Ehrenborg, M. Gustafsson, and M. Capek, "Capacity bounds and degrees of freedom for MIMO antennas constrained by Q-factor," *IEEE Trans. Antennas Propag.*, vol. 69, no. 9, pp. 5388–5400, Sep. 2021.

[64] J. C. Maxwell, "VIII. A dynamical theory of the electromagnetic field," *Phil. Trans. Roy. Soc. London*, vol. 155, pp. 459–512, 1865.

[65] W. C. Chew, *Waves and Fields in Inhomogenous Media*, vol. 16. Hoboken, NJ, USA: Wiley, 1999.

[66] J. de Rosny, G. Lerosey, and M. Fink, "Theory of electromagnetic time-reversal mirrors," *IEEE Trans. Antennas Propag.*, vol. 58, no. 10, pp. 3139–3149, Oct. 2010.

[67] S. Lin, Z. Peng, and T. M. Antonsen, "A stochastic green's function for solution of wave propagation in wave-chaotic environments," *IEEE Trans. Antennas Propag.*, vol. 68, no. 5, pp. 3919–3933, May 2020.

[68] S. Lin et al., "Predicting statistical wave physics in complex enclosures: A stochastic dyadic green's function approach," *IEEE Trans. Electromagn. Compat.*, vol. 65, no. 2, pp. 436–453, Apr. 2023.

[69] S. Lin, Z. Peng, E. Schamiloglu, Z. B. Drikas, and T. Antonsen, "A novel statistical model for the electromagnetic coupling to electronics inside enclosures," in *Proc. IEEE Int. Symp. Electromagn. Compat., Signal Power Integrity (EMC+SIPI)*, New Orleans, LA, USA, Jul. 2019, pp. 499–504.

[70] S. Lin and Z. Peng, "On the statistical analysis of space-time wave physics in complex enclosures," in *Proc. IEEE 30th Conf. Electr. Perform. Electron. Packag. Syst. (EPEPS)*, Austin, TX, USA, Oct. 2021, pp. 1–3.

[71] J.-S. Jiang and M. Ingram, "Spherical-wave model for short-range MIMO," *IEEE Trans. Commun.*, vol. 53, no. 9, pp. 1534–1541, Sep. 2005.

[72] F. Bohagen, P. Orten, and G. Oien, "On spherical vs. Plane wave modeling of line-of-sight MIMO channels," *IEEE Trans. Commun.*, vol. 57, no. 3, pp. 841–849, Mar. 2009.

[73] S. Tarboush et al., "TeraMIMO: A channel simulator for wideband ultra-massive MIMO terahertz communications," *IEEE Trans. Veh. Technol.*, vol. 70, no. 12, pp. 12325–12341, Dec. 2021.

[74] L. Han, H. Yin, and T. L. Marzetta, "Coupling matrix-based beamforming for superdirective antenna arrays," in *Proc. ICC - IEEE Int. Conf. Commun.*, May 2022, pp. 5159–5164.

[75] L. Han and H. Yin, "Superdirectivity-enhanced wireless communications: A multi-user perspective," 2023, *arXiv:2307.06958*.

[76] M. Unser, "Sampling-50 years after Shannon," *Proc. IEEE*, vol. 88, no. 4, pp. 569–587, Apr. 2000.

[77] L. Jin, X. Xu, S. Han, X. Chi, P. Zhang, and C. Yuen, "Achievable rate of linear holographic MIMO with arbitrary aperture-length," *IEEE Trans. Wireless Commun.*, vol. 23, no. 11, pp. 16742–16756, Nov. 2024.

[78] N. Mehrotra and A. Sabharwal, "When does multipath improve imaging resolution?," *IEEE J. Sel. Areas Inf. Theory*, vol. 3, no. 1, pp. 135–146, Mar. 2022.

[79] S. Loyka, "Information theory and electromagnetism: Are they related?," in *Proc. 10th ANTEM*, 2004, pp. 1–5.

[80] A. Pizzo, A. D. J. Torres, L. Sanguinetti, and T. L. Marzetta, "Nyquist sampling and degrees of freedom of electromagnetic fields," *IEEE Trans. Signal Process.*, vol. 70, pp. 3935–3947, 2022.

[81] T. J. Lim and M. Franceschetti, "Information without rolling dice," *IEEE Trans. Inf. Theory*, vol. 63, no. 3, pp. 1349–1363, Mar. 2017.

[82] M. A. Jensen and J. W. Wallace, "Capacity of the continuous-space electromagnetic channel," *IEEE Trans. Antennas Propag.*, vol. 56, no. 2, pp. 524–531, Feb. 2008.

[83] H. Landau, "On Szegö's eigenvalue distribution theorem and nonhermitian kernels," *J. D'Analyse Mathématique*, vol. 28, no. 1, pp. 335–357, 1975.

[84] D. Slepian, "Some comments on Fourier analysis, uncertainty and modeling," *SIAM Rev.*, vol. 25, no. 3, pp. 379–393, Jul. 1983.

[85] M. Franceschetti, "On Landau's eigenvalue theorem and information cut-sets," *IEEE Trans. Inf. Theory*, vol. 61, no. 9, pp. 5042–5051, Sep. 2015.

[86] R. Janaswamy, "On the EM degrees of freedom in scattering environments," *IEEE Trans. Antennas Propag.*, vol. 59, no. 10, pp. 3872–3881, Oct. 2011.

[87] M. Franceschetti, M. D. Migliore, P. Minero, and F. Schettino, "The information carried by scattered waves: Near-field and nonasymptotic regimes," *IEEE Trans. Antennas Propag.*, vol. 63, no. 7, pp. 3144–3157, Jul. 2015.

[88] J. E. Mazo, "Faster-than-nyquist signaling," *Bell Syst. Tech. J.*, vol. 54, no. 8, pp. 1451–1462, Oct. 1975.

[89] J. B. Anderson, F. Rusek, and V. Öwall, "Faster-than-nyquist signaling," *Proc. IEEE*, vol. 101, no. 8, pp. 1817–1830, Aug. 2013.

[90] T. Setälä, M. Kaivola, and A. T. Friberg, "Decomposition of the point-dipole field into homogeneous and evanescent parts," *Phys. Rev. E, Stat. Phys. Plasmas Fluids Relat. Interdiscip. Top.*, vol. 59, no. 1, pp. 1200–1206, Jan. 1999.

[91] A. Pizzo, L. Sanguinetti, and T. L. Marzetta, "Spatial characterization of electromagnetic random channels," *IEEE Open J. Commun. Soc.*, vol. 3, pp. 847–866, 2022.

[92] A. Pizzo, L. Sanguinetti, and T. L. Marzetta, "Fourier plane-wave series expansion for holographic MIMO communications," *IEEE Trans. Wireless Commun.*, vol. 21, no. 9, pp. 6890–6905, Sep. 2022.

[93] R. H. Clarke, "A statistical theory of mobile-radio reception," *Bell Syst. Tech. J.*, vol. 47, no. 6, pp. 957–1000, Jul. 1968.

[94] K. Dovelos, S. D. Assimonis, H. Q. Ngo, B. Bellalta, and M. Matthaiou, "Intelligent reflecting surfaces at terahertz bands: Channel modeling and analysis," in *Proc. IEEE Int. Conf. Commun. Workshops (ICC Workshops)*, Jun. 2021, pp. 1–6.

[95] X. Wei and L. Dai, "Channel estimation for extremely large-scale massive MIMO: Far-field, near-field, or hybrid-field?," *IEEE Commun. Lett.*, vol. 26, no. 1, pp. 177–181, Jan. 2022.

[96] L. Wei et al., "Tri-polarized holographic MIMO surfaces for near-field communications: Channel modeling and precoding design," *IEEE Trans. Wireless Commun.*, vol. 22, no. 12, pp. 8828–8842, Dec. 2023.

[97] A. A. Glazunov, M. Gustafsson, A. F. Molisch, F. Tufvesson, and G. Kristensson, "Spherical vector wave expansion of Gaussian electromagnetic fields for antenna-channel interaction analysis," *IEEE Trans. Antennas Propag.*, vol. 57, no. 7, pp. 2055–2067, Jul. 2009.

[98] A. A. Glazunov, M. Gustafsson, A. F. Molisch, and F. Tufvesson, "Physical modelling of multiple-input multiple-output antennas and channels by means of the spherical vector wave expansion," *IET Microw., Antennas Propag.*, vol. 4, no. 6, pp. 778–791, Jun. 2010.

[99] J. An, C. Yuen, C. Huang, M. Debbah, H. V. Poor, and L. Hanzo, "A tutorial on holographic MIMO communications—Part I: Channel modeling and channel estimation," *IEEE Commun. Lett.*, vol. 27, no. 7, pp. 1664–1668, Jul. 2023.

[100] T. Gong, L. Wei, C. Huang, G. C. Alexandropoulos, M. Debbah, and C. Yuen, "Near-field channel modeling for holographic MIMO communications," *IEEE Wireless Commun.*, vol. 31, no. 3, pp. 108–116, Jun. 2024.

Authorized licensed use limited to: Zhejiang University. Downloaded on May 24,2026 at 03:23:22 UTC from IEEE Xplore. Restrictions apply.

[101] A. Pizzo, T. L. Marzetta, and L. Sanguinetti, "Spatially-stationary model for holographic MIMO small-scale fading," *IEEE J. Sel. Areas Commun.*, vol. 38, no. 9, pp. 1964–1979, Sep. 2020.
[102] *Holographic-Mimo-Small-Scale-Fading*. Accessed: Apr. 5, 2025. [Online]. Available: https://github.com/lucasanguinetti/Holographic-MIMO-Small-Scale-Fading
[103] L. Wei et al., "Electromagnetic channel modeling and capacity analysis for HMIMO communications," *IEEE Trans. Wireless Commun.*, vol. 24, no. 5, pp. 4500–4514, May 2025.
[104] S. Lin, Y. Shao, and Z. Peng, "On the vectorial property of stochastic dyadic green's function in complex electronic enclosures," in *Proc. IEEE Int. Symp. Electromagn. Compat. Signal/Power Integrity (EMCSI)*, Aug. 2022, pp. 350–355.
[105] S. Lin, E. Dohme, and Z. Peng, "A stochastic green's function–integral equation method for communication in diffuse multipath environments," in *Proc. Int. Conf. Electromagn. Adv. Appl. (ICEAA)*, Cartagena, Colombia, Sep. 2018, pp. 567–570.
[106] H. Do, N. Lee, and A. Lozano, "Line-of-sight MIMO via intelligent reflecting surface," *IEEE Trans. Wireless Commun.*, vol. 22, no. 6, pp. 4215–4231, Jun. 2023.
[107] D. Dardari, "Communicating with large intelligent surfaces: Fundamental limits and models," *IEEE J. Sel. Areas Commun.*, vol. 38, no. 11, pp. 2526–2537, Nov. 2020.
[108] N. Decarli and D. Dardari, "Communication modes with large intelligent surfaces in the near field," *IEEE Access*, vol. 9, pp. 165648–165666, 2021.
[109] G. Iacovelli, C. Iacovelli, and S. Chatzinotas, "Holographic MIMO surfaces: A channel model approximation in the electromagnetic domain," *IEEE Wireless Commun. Lett.*, vol. 14, no. 2, pp. 305–309, Feb. 2025.
[110] R. Pierri and F. Soldovieri, "On the information content of the radiated fields in the near zone over bounded domains," *Inverse Problems*, vol. 14, no. 2, pp. 321–337, Apr. 1998.
[111] A. M. Sayeed, "Deconstructing multiantenna fading channels," *IEEE Trans. Signal Process.*, vol. 50, no. 10, pp. 2563–2579, Oct. 2002.
[112] B. Wang et al., "Spatial-wideband effect in massive MIMO with application in mmWave systems," *IEEE Commun. Mag.*, vol. 56, no. 12, pp. 134–141, Dec. 2018.
[113] Z. Wu and L. Dai, "The manifestation of spatial wideband effect in circular array: From beam split to beam defocus," *IEEE Trans. Commun.*, vol. 72, no. 5, pp. 3064–3078, May 2024.
[114] B. Wang, F. Gao, S. Jin, H. Lin, and G. Y. Li, "Spatial- and frequency-wideband effects in millimeter-wave massive MIMO systems," *IEEE Trans. Signal Process.*, vol. 66, no. 13, pp. 3393–3406, Jul. 2018.
[115] Z. Wang, X. Mu, and Y. Liu, "Rethinking integrated sensing and communication: When near field meets wideband," *IEEE Commun. Mag.*, vol. 62, no. 9, pp. 44–50, Sep. 2024.
[116] J. C. Ruiz-Sicilia, M. Di Renzo, M. D. Migliore, M. Debbah, and H. V. Poor, "On the degrees of freedom and eigenfunctions of line-of-sight holographic MIMO communications," 2025, *arXiv:2308.08009*.
[117] A. Pizzo, T. L. Marzetta, and L. Sanguinetti, "Degrees of freedom of holographic MIMO channels," in *Proc. IEEE 21st Int. Workshop Signal Process. Adv. Wireless Commun. (SPAWC)*, May 2020, pp. 1–5.
[118] L. Wei et al., "Multi-user holographic MIMO surfaces: Channel modeling and spectral efficiency analysis," *IEEE J. Sel. Topics Signal Process.*, vol. 16, no. 5, pp. 1112–1124, Aug. 2022.
[119] S. Yue, L. Liu, and B. Di, "Directivity-aware degrees of freedom analysis for extremely large-scale MIMO," *IEEE Trans. Veh. Tech.*, vol. 74, no. 6, pp. 9950–9954, Jun. 2025.
[120] Z. Wang et al., "Analytical framework for effective degrees of freedom in near-field XL-MIMO," *IEEE Trans. Wireless Commun.*, vol. 24, no. 4, pp. 3465–3482, Apr. 2025.
[121] C. Ehrenborg and M. Gustafsson, "Physical bounds and radiation modes for MIMO antennas," *IEEE Trans. Antennas Propag.*, vol. 68, no. 6, pp. 4302–4311, Jun. 2020.
[122] A. S. de Sena et al., "IRS-assisted massive MIMO-NOMA networks: Exploiting wave polarization," *IEEE Trans. Wireless Commun.*, vol. 20, no. 11, pp. 7166–7183, Nov. 2021.
[123] F. Zhu et al., "Beamforming inferring by conditional WGAN-GP for holographic antenna arrays," *IEEE Wireless Commun. Lett.*, vol. 13, no. 7, pp. 2023–2027, Jul. 2024.
[124] J. An, C. Yuen, C. Huang, M. Debbah, H. V. Poor, and L. Hanzo, "A tutorial on holographic MIMO communications—Part II: Performance analysis and holographic beamforming," *IEEE Commun. Lett.*, vol. 27, no. 7, pp. 1669–1673, Jul. 2023.
[125] *Electromagnetic Information—Kolmogorov*. Accessed: Apr. 5, 2025. [Online]. Available: https://sites.google.com/unicas.it/electromagnetic-information/download/programs/kolmogorov
[126] Y. Cheng, W. Peng, C. Huang, G. C. Alexandropoulos, C. Yuen, and M. Debbah, "RIS-aided wireless communications: Extra degrees of freedom via rotation and location optimization," *IEEE Trans. Wireless Commun.*, vol. 21, no. 8, pp. 6656–6671, Aug. 2022.
[127] Y. Zhang, J. Zhang, Y. Zhang, Y. Yao, and G. Liu, "Capacity analysis of holographic MIMO channels with practical constraints," *IEEE Wireless Commun. Lett.*, vol. 12, no. 6, pp. 1101–1105, Jun. 2023.
[128] M. D. Migliore, "On the sampling of the electromagnetic field radiated by sparse sources," *IEEE Trans. Antennas Propag.*, vol. 63, no. 2, pp. 553–564, Feb. 2015.
[129] S. S. A. Yuan, Z. He, S. Sun, X. Chen, C. Huang, and W. E. I. Sha, "Electromagnetic effective-degree-of-freedom limit of a MIMO system in 2-D inhomogeneous environment," *Electronics*, vol. 11, no. 19, p. 3232, Oct. 2022. [Online]. Available: https://www.mdpi.com/2079-9292/11/19/3232
[130] R. Li et al., "An electromagnetic information theory based model for efficient characterization of MIMO systems in complex space," *IEEE Trans. Antennas Propag.*, vol. 71, no. 4, pp. 3497–3508, Apr. 2023.
[131] Y. Shen, Z. He, W. E. I. Sha, S. S. A. Yuan, and X. Chen, "Electromagnetic effective-degree-of-freedom prediction with parabolic equation method," *IEEE Trans. Antennas Propag.*, vol. 71, no. 4, pp. 3752–3757, Apr. 2023.

Li Wei (Member, IEEE) received the B.Sc. degree in communication engineering from Southwest Jiaotong University, China, in 2015, the M.Sc. degree in electronic and communication engineering from Xidian University, China, in 2019, and the Ph.D. degree from Singapore University of Technology and Design, Singapore, in 2023. She is currently a Research Fellow with the School of Electrical and Electronic Engineering, Nanyang Technological University, Singapore. Her research interests include holographic MIMO communications, reconfigurable intelligent surfaces, and signal processing for wireless communications.

Tierui Gong (Member, IEEE) received the Ph.D. degree from the University of Chinese Academy of Sciences, Beijing, China, in 2020. He is a Research Fellow with the School of Electrical and Electronic Engineering, Nanyang Technological University (NTU), Singapore. From June 2018 to May 2019, he was a Visiting Student with the Faculty of Electrical Engineering, Technion—Israel Institute of Technology, and then with the Faculty of Mathematics and Computer Science, Weizmann Institute of Science, Israel. He was a Special Research Associate with the Institute of Computing Technology, Chinese Academy of Sciences, Beijing, China, from 2020 to 2021. He was a Research Fellow with the Engineering Product Development Pillar, Singapore University of Technology and Design, Singapore, from 2022 to 2023. He is the Co-Principal Investigator and a Lead Scientist of several projects at the intersection of quantum information technology and wireless communications, supported by prestigious funding agencies, including the Ministry of Education, Singapore, and Temasek Laboratories. His research interests include quantum information technologies for advanced wireless communication/sensing systems, Rydberg neutral atom empowered wireless systems, holographic MIMO and massive MIMO for 6G, electromagnetic signal, and information theory. He is serving as the Lead Workshop Chair for IEEE PIMRC 2026 and the Lead Guest Editor for *Electronics* special issue. He has served as a TPC member for several prestigious IEEE conferences and a reviewer for a list of top-tier journals.

Authorized licensed use limited to: Zhejiang University. Downloaded on May 24,2026 at 03:23:22 UTC from IEEE Xplore. Restrictions apply.

Chongwen Huang (Senior Member, IEEE) received the B.Sc. degree from Nankai University in 2010, the M.Sc. degree from the University of Electronic Science and Technology of China in 2013, and the Ph.D. degree from Singapore University of Technology and Design (SUTD) in 2019. From October 2019 to September 2020, he was a Post-Doctoral Researcher with SUTD. In September 2020, he joined Zhejiang University, as a tenure-track Young Professor. His main research interests are focused on holographic MIMO surface/reconfigurable intelligent surface, B5G/6G wireless communications, mmWave/THz communications, deep learning technologies for wireless communications. He was a recipient of the 2021 IEEE Marconi Prize Paper Award, the 2023 IEEE Fred W. Ellersick Prize Paper Award, and the 2021 IEEE ComSoc Asia–Pacific Outstanding Young Researcher Award. He has been served as an Editor for IEEE COMMUNICATIONS LETTER, *Signal Processing* (Elsevier), *EURASIP Journal on Wireless Communications and Networking*, and *Physical Communication* since 2021.

Zhaoyang Zhang (Senior Member, IEEE) received the Ph.D. degree from Zhejiang University, Hangzhou, China, in 1998.

He is currently a Qiushi Distinguished Professor with Zhejiang University. He has co-authored more than 200 IEEE journal articles. His current research interests are mainly focused on AI-empowered communications and networking, intelligent and integrated communication, sensing and computing, information theory, and computation theory. He was a co-recipient of the 2024 IEEE Leonard G. Abraham Prize; and over ten Best Paper Awards, the Best Student Paper Awards, and the Student Travel Award of IEEE ICC 2019, Globecom 2020, ISIT 2023, WCNC 2024, and PIMRC 2025. He received the National Natural Science Fund for Distinguished Young Scholar by NSFC in 2017. He was also a co-recipient of the First Grade State-Level Award for Graduate Teaching and Education in 2023. He was the General Co-Chair and the TPC Co-Chair of WCSP 2023/2018/2013, PIMRC 2021 Workshop on Native AI Empowered Wireless Networks, and VTC-Spring 2017 Workshop on HMWC. He was also a keynote speaker of IEEE Globecom 2021 Workshop on Native-AI, APCC 2018, and VTC-Fall 2017 Workshop on NOMA. He served as an Editor for IEEE TRANSACTIONS ON WIRELESS COMMUNICATIONS and IEEE TRANSACTIONS ON COMMUNICATIONS and the Lead Guest Editor for IEEE WIRELESS COMMUNICATIONS Special Issue on Sustainable Big AI Model for Wireless Networks.

Wei E. I. Sha (Fellow, IEEE) received the Ph.D. degree in electromagnetic fields and microwave technology from Anhui University, Hefei, China, in 2008.

From 2008 to 2017, he was with the Department of Electrical and Electronic Engineering, The University of Hong Kong, where he was a Post-Doctoral Research Fellow and later as a Research Assistant Professor. From 2018 to 2019, he was a Marie Skłodowska-Curie Individual Fellow with University College London, U.K. He is currently a tenured Associate Professor with the College of Information Science and Electronic Engineering, Zhejiang University, Hangzhou, China, where he is the Deputy Director of the Institute of Electromagnetic Information and Electronic Integration. He has authored or co-authored two books, ten book chapters, and over 220 peer-reviewed journal articles. His works have been cited over 13 770 times on Google Scholar with an H-index of 62. His research interests include theoretical and applied electromagnetics, with a focus on computational electromagnetics, quantum electromagnetics, and electromagnetic information theory.

Dr. Sha received the ACES Technical Achievement Award in 2022, the Second Prize of Science and Technology Award of the China Institute of Communications in 2024, the Second Prize for Science and Technology from the Anhui Provincial Government in 2015, and 11 international conference paper awards. He is the Founding Chair of the IEEE Antennas and Propagation Society (AP-S) Zhejiang Chapter. He served as an Associate Editor for IEEE JOURNAL ON MULTISCALE AND MULTIPHYSICS COMPUTATIONAL TECHNIQUES, IEEE OPEN JOURNAL OF ANTENNAS AND PROPAGATION, and *Electromagnetic Science*.

Zhi Ning Chen (Fellow, IEEE) received the B.Eng., M.Eng., and Ph.D. degrees in electrical engineering from the Institute of Communications Engineering (ICE), China, in 1985, 1988, and 1993, respectively, and the second Ph.D. degree from the University of Tsukuba, Japan, in 2003.

From 1988 to 1997, he was with ICE, Southeast University, and the City University of Hong Kong. He conducted research at the University of Tsukuba during (1997–1999) and visited the University again in 2001 and 2004, all sponsored by Japan Society for the Promotion of Science Fellowship Programs. In 2004, he was an Academic Visitor with the IBM Watson Research Center, Yorktown. In 2013, he visited "Laboratoire des SignauxetSystémes," UMR8506 CNRS–Supelec–University Paris Sud, Gif-sur-Yvette, France, as a Senior DIGITEO Guest Scientist. In 2015, he visited the Center for Northeast Asian Studies, Tohoku University, Japan, as a Senior Visiting Professor. From 1999 to 2016, he was with the Institute for Infocomm Research, Singapore, in various capacities, including a Principal Scientist, the Department Head, the Manager, and a Technical Advisor. In 2012, he joined the Department of Electrical and Computer Engineering, National University of Singapore, as a Provost's Chair Professor. He was appointed as the Industry Program Director and the Director of the Advanced Research and Technology Innovation Centre. He has/held concurrent guest professorships at more than 15 local and overseas universities, and has provided consultancy services to local and overseas companies, as a Technical Advisor, a Guest Professor, and a Chief Scientist. He has delivered more than 180 keynote, plenary, and invited speeches at international events. He has published 760 papers and six books titled *Broadband Planar Antennas* (Wiley, 2005), *UWB Wireless Communication* (Wiley, 2006), *Antennas for Portable Devices* (Wiley, 2007), *Antennas for Base Stations in Wireless Communications* (McGraw-Hill, 2009), *Handbook of Antenna Technologies* (Springer References, 2016; 76 chapters; Editor-in-Chief), and *Substrate-Integrated Millimeter-Wave Antennas for Next-Generation Communications and Radars* (Wiley and IEEE Press, 2021), in addition to nine chapters in other books. He holds 36 granted and filed patents and has completed 43 licensing deals with industry. His current interests include translational research of electromagnetic metamaterials and the application of prior-knowledge-guided machine learning-enabled algorithms to antenna engineering.

Dr. Chen was elevated to fellow of the Academy of Engineering, Singapore, in 2019 and to a fellow of IEEE in 2007 for contributions to small and broadband antennas for wireless applications. He was a recipient of the EurAAP Antenna Award 2025, the IEEE Antennas and Propagation Society John Kraus Antenna Award 2021, the ASEAN Outstanding Engineering Achievement Award 2013, the Institution of Engineers Singapore Prestigious Engineering Achievement Awards in 2006, 2013 (two awards), and 2014, and more than 35 best paper awards with his students. He is the Founding General Chair of the International Workshop on Antenna Technology in 2005, the International Symposium on InfoComm and Mechatronics Technology in Bio-Medical and Healthcare Application in 2010, the International Microwave Forum in 2010, Asia–Pacific Conference on Antennas and Propagation in 2012, and the Marina Forum in 2021. He served as the General Chair for the 2021 IEEE International Symposium on Antennas and Propagation and USNC-URSI Radio Science Meeting. He served on the IEEE Council on RFID as a Distinguished Lecturer and as a Founding Vice President (2015–2020). He served as the Chair for the IEEE Singapore MTT/AP Chapter in 2008 and the Founding Chair for the IEEE Singapore RFID Chapter from 2016 to 2017. He serves on IEEE TRANSACTIONS ON ANTENNAS AND PROPAGATION as an Associate Editor. He has served on the IEEE Antennas and Propagation Society as a Distinguished Lecturer; and a member of the AdCom Committee, Fellow Committee, and New Directions Committee.

Authorized licensed use limited to: Zhejiang University. Downloaded on May 24,2026 at 03:23:22 UTC from IEEE Xplore. Restrictions apply.

Linglong Dai (Fellow, IEEE) received the B.S. degree from Zhejiang University, Hangzhou, China, in 2003, the M.S. degree (Hons.) from China Academy of Telecommunications Technology, Beijing, China, in 2006, and the Ph.D. degree (Hons.) from Tsinghua University, Beijing, in 2011. From 2011 to 2013, he was a Post-Doctoral Research Fellow with the Department of Electronic Engineering, Tsinghua University, where he was an Assistant Professor from 2013 to 2016 and an Associate Professor from 2016 to 2022. Since 2022, he has been a Professor with Tsinghua University. He has co-authored the book *mmWave Massive MIMO: A Paradigm for 5G* (Academic Press, 2016). He has authored or co-authored over 90 IEEE journal articles and over 50 IEEE conference papers. He also holds over 20 granted patents. His current research interests include massive MIMO, reconfigurable intelligent surface (RIS), millimeter-wave and terahertz communications, machine learning for wireless communications, near-field communications, and quantum information technologies. He has received the five IEEE Best Paper Awards at IEEE ICC 2013, IEEE ICC 2014, IEEE ICC 2017, IEEE VTC 2017-Fall, and IEEE ICC 2018. He has also received the Tsinghua University Outstanding Ph.D. Graduate Award in 2011, the Beijing Excellent Doctoral Dissertation Award in 2012, the China National Excellent Doctoral Dissertation Nomination Award in 2013, the URSI Young Scientist Award in 2014, the IEEE Transactions on Broadcasting Best Paper Award in 2015, the Electronics Letters Best Paper Award in 2016, the National Natural Science Foundation of China for Outstanding Young Scholars in 2017, the IEEE ComSoc Asia–Pacific Outstanding Young Researcher Award in 2017, the IEEE ComSoc Asia–Pacific Outstanding Paper Award in 2018, the China Communications Best Paper Award in 2019, the IEEE Access Best Multimedia Award in 2020, the IEEE Communications Society Leonard G. Abraham Prize in 2020, the IEEE ICC Outstanding Demo Award in 2022, the National Science Foundation for Distinguished Young Scholars in 2023, and the IEEE ComSoc Stephen O. Rice Prize in 2025. He was listed as a Highly Cited Researcher by Clarivate Analytics from 2020 to 2025.

Mérouane Debbah (Fellow, IEEE) is currently a Professor with the Khalifa University of Science and Technology, Abu Dhabi; and the Founding Senior Director of KU Digital Future Institute. His research has been lying at the interface of fundamental mathematics, algorithms, statistics, information, and communication sciences, with a special focus on random matrix theory and learning algorithms. In the communication field, he has been with the heart of the development of small cells (4G), massive MIMO (5G), and large intelligent surfaces (6G) technologies. In the AI field, he is known for his work on large language models, distributed AI systems for networks, and semantic communications. He is a WWRF Fellow, a Eurasip Fellow, an AAIA Fellow, an Institut Louis Bachelier Fellow, an AIIA Fellow, and a Membre émérite SEE. He received multiple prestigious distinctions, prizes, and best paper awards (more than 50 IEEE best paper awards) for his contributions to both. He is the Actually Chair of the IEEE Large Generative AI Models in Telecom (GenAINet) Emerging Technology Initiative and a member of the Marconi Prize Selection Advisory Committee.

Chau Yuen (Fellow, IEEE) received the B.Eng. and Ph.D. degrees from Nanyang Technological University, Singapore, in 2000 and 2004, respectively. He was a Post-Doctoral Fellow with Lucent Technologies Bell Laboratories, Murray Hill, in 2005. From 2006 to 2010, he was with the Institute for Infocomm Research, Singapore. From 2010 to 2023, he was with the Engineering Product Development Pillar, Singapore University of Technology and Design. Since 2023, he has been with the School of Electrical and Electronic Engineering, Nanyang Technological University, currently he is the Provost's Chair in Wireless Communications, the Assistant Dean in Graduate College, and the Cluster Director for Sustainable Built Environment with ER@IN. He received the IEEE Communications Society Leonard G. Abraham Prize in 2024, the IEEE Communications Society Best Tutorial Paper Award in 2024, the IEEE Communications Society Fred W. Ellersick Prize in 2023, the IEEE Marconi Prize Paper Award in Wireless Communications in 2021, the IEEE APB Outstanding Paper Award in 2023, and the EURASIP Best Paper Award for *Journal on Wireless Communications and Networking* in 2021. He also serves as an Editor for IEEE TRANSACTIONS ON VEHICULAR TECHNOLOGY, IEEE TRANSACTIONS ON NEURAL NETWORKS AND LEARNING SYSTEMS, and IEEE TRANSACTIONS ON NETWORK SCIENCE AND ENGINEERING, where he was awarded as IEEE Transactions on Network Science and Engineering Excellent Editor Award, in 2025, 2024, and 2022; and a Top Associate Editor for IEEE TRANSACTIONS ON VEHICULAR TECHNOLOGY from 2009 to 2015. He is listed as a Top 2% Scientists by Stanford University and also a Highly Cited Researcher by Clarivate Web of Science from 2022.

Authorized licensed use limited to: Zhejiang University. Downloaded on May 24,2026 at 03:23:22 UTC from IEEE Xplore. Restrictions apply.